COMILLAS
UNIVERSIDAD PONTIFICIA
ICAI

GRADO EN INGENIERÍA EN TECNOLOGÍAS INDUSTRIALES

BACHELOR'S DEGREE FINAL PROJECT

"Optimizing Laser-Based Powder Bed Fusion Parameters for Dense Builds in Metal Additive Manufacturing: A Study on 316L Stainless Steel Using Aconity3D Micro L-PBF Machine"

Author: Ramón Durán Alonso

Advisor: Mostafa Hassani

Madrid

I declare, under my responsibility, that the Project presented with the title

"Optimizing Laser-Based Powder Bed Fusion Parameters for Dense Builds in Metal Additive Manufacturing: A Study on 316L Stainless Steel Using Aconity3D Micro L-PBF Machine"

in the ETS of Engineering - ICAI of the Universidad Pontificia Comillas in the

2023/2024 academic year is my authorship, original and unpublished and

It has not been previously submitted for other purposes.

This project has not been plagiarized, totally or partially, and the information

That has been taken from other documents is duly referenced

Signed: Ramón Durán Alonso Date: ……/ July / 2024

Project delivery authorized

THE PROJECT ADVISOR

Signed: Mostafa Hassani Date: ……/ July / 2024

GRADO EN INGENIERÍA EN TECNOLOGÍAS INDUSTRIALES

TRABAJO DE FIN DE GRADO

“Optimizing Laser-Based Powder Bed Fusion Parameters for Dense Builds in Metal Additive Manufacturing: A Study on 316L Stainless Steel Using Aconity3D Micro L-PBF Machine”

Autor: Ramón Durán Alonso

Director: Mostafa Hassani

Madrid

Acknowledgement

I would like to express my sincere gratitude to Cornell University Faculty, specially to Professor Mostafa Hassani, for providing me the great opportunity to work hands on hands with other fantastic and driven students who were part of the Hassani research group at the Sibley School of Mechanical and Aerospace Engineering.

A special thank you to Justin Wan for his invaluable support, advice and guidance as colleague during my time as a member of the group and throughout the development of this project.

Optimizing Laser-based Powder Bed Fusion Parameters for Dense Builds in Metal Additive Manufacturing: A Study on 316l Stainless Steel Using Aconity3D Micro L-PBF Machine.

Author: Durán Alonso, Ramón.
Advisor: Hassani, Mostafa.
Collaborating Entity: ICAI – Universidad Pontificia Comillas, and Cornell University

ABSTRACT

Upon the acquisition of the AconityMICRO compact laser powder bed fusion system by Cornell University, a necessity for a solid foundation to ensure constant high density and quality builds rose. The objective of this project is to provide a framework of sensibly chosen processing parameters based on the extensive literature available on analogous processes on 316L stainless steel. Basing on the energy density approach, a processing map is constructed with the ability to predict defect formation on future sample manufacturing with the AconityMICRO. In parallel, a similar study to predict the microstructural characteristics of future samples is conducted along with learning the necessary steps to properly manipulate the machine and perform a post-processing analysis.

Keywords: Laser powder bed fusion, 316L stainless steel, processing parameters optimization, porosity defects, microstructure.

1. Introduction

Additive manufacturing has recently surged in popularity due to its versatility in design and its ability to produce highly customizable parts from 3D models. This surge has been especially notable in metal fabrication, where AM can create structures with high geometrical complexity and performance efficiently, reducing time, costs, and material waste. This capability has awakened great interest from industries like energy, defense, and aerospace, where such components were previously unattainable through traditional manufacturing methods.

Laser Powder Bed Fusion (LPBF) stands out as particularly promising within the metal AM scope and is the focus of this project. In LPBF, powder feedstock is spread as a powder bed layer and selectively melted by a heat laser source to build components layer by layer, enabling the creation of intricate geometries. However, LPBF faces challenges such as porosity, inclusions, and residual stress, influenced by processing parameters like laser

power, scanning speed, hatch spacing, and layer thickness. Optimizing these parameters is crucial to ensure parts meet performance and quality requirements.

2. Project definition

This project aims to establish a reliable framework that ensures the validity and reliability of new scientific endeavors using the LPBF machine at Cornell University. The primary objective is to develop a coherent parameter set that minimizes part defects. The second goal is to understand the microstructural characteristics of additively manufactured 316L stainless steel through LPBF processes.

Achieving these objectives requires three parallel steps: acquiring a thorough understanding of the AconityMICRO machine through professional training, mastering the use of Netfabb and Fusion 360 software for part parameter transmission and design, and conducting comprehensive characterization of the manufactured parts. This characterization involves polishing the parts and posterior evaluation with electronic microscopy to analyze porosity defects and primary grain characteristics.

3. System description

This study involves a comprehensive review of existing literature on similar LPBF processes, including experimental studies, analytical solutions, and predictive models. The processing parameter sets are tailored to the specific type of powder used with the AconityMICRO machine at Cornell, forming a robust foundation for future scientific investigations. Parameter-specific maps based on the Volumetric Energy Density (VED) as shown in *Figure 1* and other relevant metrics will illustrate the relationship between power and scan speed, aiming to provide a deep understanding of the expected outcomes for each chosen parameter set and trying to minimize the occurrence of lack of fusion and keyhole defects.

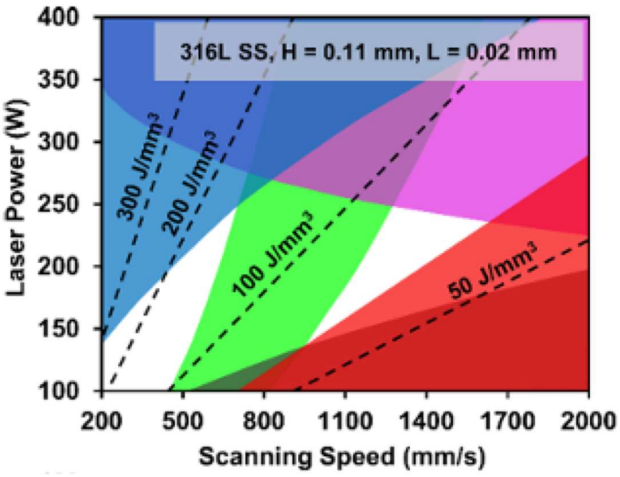

Figure 1: VED based processing map for 316L alloy [2]

For the microstructure prediction, analytical methods on solidification dynamics and experimental validations to predict the size and morphology of grain structures will be provided, as shown in *Figure 2*. An accurate previous prediction of columnar or equiaxed grains is crucial for determining the final mechanical properties and performance of the parts.

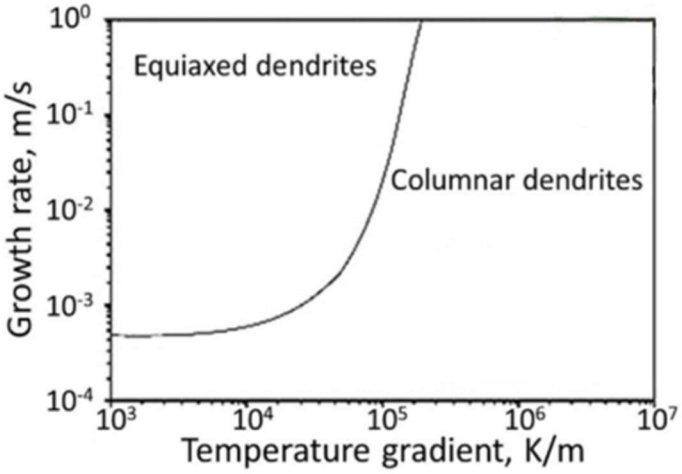

Figure 2: Transition from columnar to equiaxed grains based on G and R

4. Results

The analysis of the most relevant published literature to date, plotted in *Figure 3*, indicated that VED values between 65 and 100 J/mm³ are ideal for achieving high-density samples. Notably, specific overlapping VED ranges such as 100 to 125 J/mm³ and 45 to 65 J/mm³, on different papers, revealed zones where optimal density coexisted with defects like keyhole and LOF porosity. To capitalize on this insight, the recommended parameters by this study for the AconityMICRO system include a layer thickness of 30 µm and a hatch spacing of

0.080 mm. These settings are anticipated to provide the broadest optimal processing window, balancing high density with minimal defects.

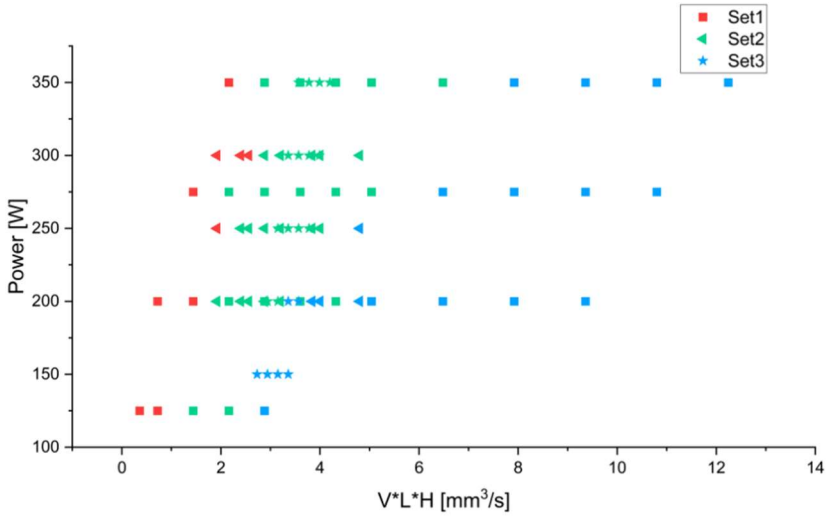

Figure 3: Plot of most relevant literature references

Training and preparation were critical components of this project. Students at Cornell University received extensive training sessions led by industry specialists. These sessions encompassed machine operation, safety protocols, digital interface manipulation, and powder handling. Furthermore, students were instructed to use software tools like Netfabb and Fusion 360 to design and model parts. Post-processing techniques, including polishing and microscopy imaging, were also practiced to analyze fabricated samples thoroughly. This comprehensive training ensures that students are well-prepared to independently operate the AconityMICRO system and apply their knowledge effectively in future research.

5. Conclusions

The conclusion of the study highlights two key aspects: The first aspect focuses on achieving a high density set of components made from 316L stainless steel by combining analytical solutions and published studies to establish critical processing parameters. These parameters, derived from the energy density approach, maximize the optimal processing window and predict defect formation. The established ranges of VED provide a robust framework for defect prediction, and in combination with microstructure anticipation, both are crucial for the success of the future LPBF builds.

The second aspect involves the necessary steps to ensure proper functioning and manipulation of the LPBF system at Cornell. This includes translating information from CAD models to the machine's software and mastering post-processing procedures. Possible

future validation of the established parameter maps' accuracy and applicability involves creating and analyzing samples to verify the VED Map. The proposed method includes producing 15 testing samples, with parameters distributed across optimal, transition, and defect-prone zones. This validation process, combined with training sessions and post-processing techniques, ensures the AconityMICRO's reliable operation and prepares engineers for future work with the machine.

6. References

[1] Oliveira, J. P., LaLonde, A. D., & Ma, J. (2020). Processing parameters in laser powder bed fusion metal additive manufacturing. Materials & Design, 193, 108762.

[2] Agrawal, A. K., Rankouhi, B., & Thoma, D. J. (2022). Predictive process mapping for laser powder bed fusion: A review of existing analytical solutions. Current Opinion in Solid State and Materials Science, 26(6), 101024.

[3] Yakout, M., Elbestawi, M. A., & Veldhuis, S. C. (2019). Density and mechanical properties in selective laser melting of invar 36 and stainless steel 316L. Journal of Materials Processing Technology, 266, 397-420

[4] Diaz Vallejo, N.; Lucas, C.; Ayers, N.; Graydon, K.; Hyer, H.;Sohn, Y. Process Optimization and Microstructure Analysis to Understand Laser Powder Bed Fusion of 316L Stainless Steel. Metals 2021,11, 832

Optimizing Laser-based Powder Bed Fusion Parameters for Dense Builds in Metal Additive Manufacturing: A Study on 316l Stainless Steel Using Aconity3D Micro L-PBF Machine.

Autor: Durán Alonso, Ramón.
Director: Hassani, Mostafa.
Entidad Colaboradora: ICAI – Universidad Pontificia Comillas, y Cornell University.

RESUMEN DEL PROYECTO

Con la adquisición del sistema compacto de fusión por lecho de polvo láser (LPBF) AconityMICRO por parte de la Universidad de Cornell, surge la necesidad de una crear un marco para garantizar la fabricación de piezas alta densidad y calidad con esta máquina. El objetivo de este proyecto es proporcionar dicho marco de parámetros de procesamiento elegidos de manera sensata, basados en los extensos estudios disponibles sobre procesos análogos en acero inoxidable 316L. Basándose en el enfoque de densidad de energía volumétrica (VED), se ha construido un mapa para predecir la formación de defectos en la fabricación de muestras futuras con la AconityMICRO. Paralelamente, se ha llevado a cabo un estudio similar para predecir las características de la microestructura que se puede esperar, junto con el aprendizaje de los pasos necesarios para manipular correctamente la máquina y realizar un análisis posterior al procesamiento de las piezas que se fabriquen.

Palabras Clave: Fusión por lecho de polvo láser, acero inoxidable 316L, optimización de parámetros de procesamiento, defectos por porosidad, microestructura.

1. Introducción

La fabricación aditiva ha aumentado en popularidad recientemente debido a su versatilidad en el diseño y su capacidad para producir piezas altamente personalizables a partir de modelos 3D. Este aumento ha sido especialmente notable en la fabricación con metales, donde se pueden crear estructuras de alta complejidad geométrica y rendimiento de manera eficiente, reduciendo tiempo, coste y desperdicio de material. Esta capacidad ha despertado gran interés en industrias como la energética, defensa y aeroespacial, donde dichas metas eran antes inalcanzables a través de métodos de fabricación tradicionales.

La fusión por lecho de polvo láser (LPBF) destaca especialmente dentro del ámbito de la manufactura aditiva de metales y será el tema principal de este proyecto. En LPBF, el material en polvo se extiende en una capa fina y se funde mediante una fuente de calor láser para así construir piezas capa por capa, permitiendo la creación de geometrías muy

complejas. Sin embargo, el LPBF se enfrenta desafíos como la porosidad, inclusiones y tensiones residuales, influenciados por parámetros de procesamiento como la potencia del láser, la velocidad de escaneo, la distancia entre pasadas del láser y el espesor de capa de polvo. Optimizar estos parámetros es clave a la hora de asegurar que las piezas cumplan con los requisitos de rendimiento y calidad exigidos.

2. Definición del Proyecto

Este proyecto tiene como objetivo establecer un marco de confianza que asegure la fiabilidad de futuros proyectos científicos utilizando la máquina aconityMICRO en la Universidad de Cornell. El objetivo principal es desarrollar un conjunto coherente de parámetros que minimicen los defectos en las piezas. El segundo objetivo es comprender la microestructura y sus características principales para las piezas de acero inoxidable 316L fabricadas a través de procesos LPBF.

Lograr estos objetivos requiere tres pasos paralelos: adquirir una formación completa sobre el funcionamiento de la máquina AconityMICRO a través de un entrenamiento, dominar el uso del software Netfabb y Fusion 360 para la transmisión y diseño de parámetros de piezas, y realizar una caracterización exhaustiva post-fabricación de las piezas fabricadas. Esta caracterización incluye el pulido de las piezas y la evaluación posterior a través de microscopio electrónico para analizar defectos de porosidad y características de grano.

3. Descripción del modelo/sistema/herramienta

Este proyecto se basa en una revisión exhaustiva de los estudios existentes sobre procesos similares de LPBF, incluyendo estudios experimentales, soluciones analíticas y modelos predictivos. Los conjuntos de parámetros de procesamiento elegidos se adaptan al tipo específico de polvo utilizado con la máquina AconityMICRO en Cornell, creando así un marco sólido para futuras investigaciones científicas. Los mapas de parámetros basados en la densidad de energía volumétrica (VED), como aparece en la *Figura 1*, junto con otras métricas relevantes muestran la relación entre la potencia y la velocidad de escaneo, con el objetivo de proporcionar visión clara de los resultados esperados para cada conjunto de parámetros elegido y tratar de minimizar la ocurrencia de defectos de “lack of fusion” y de “keyhole”.

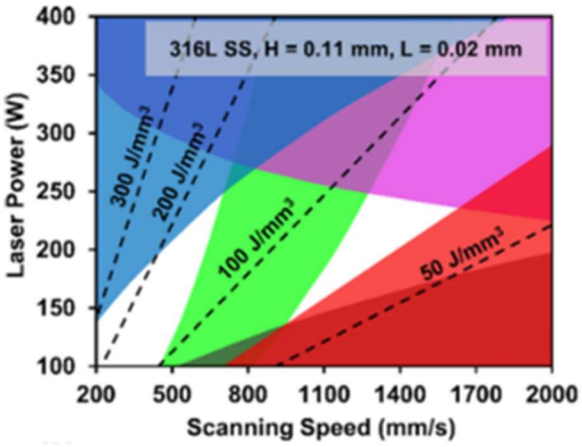

Figure 1: VED based processing map for 316L alloy [2]

Para la predicción de la microestructura, se han proporcionado métodos analíticos sobre la dinámica de solidificación, así como experimentos publicados, para predecir el tamaño y la morfología de las estructuras granulares, como mostrado en la *Figura 2*. Una predicción precisa del tipo de grano es crucial para determinar las propiedades mecánicas finales y el rendimiento de las piezas.

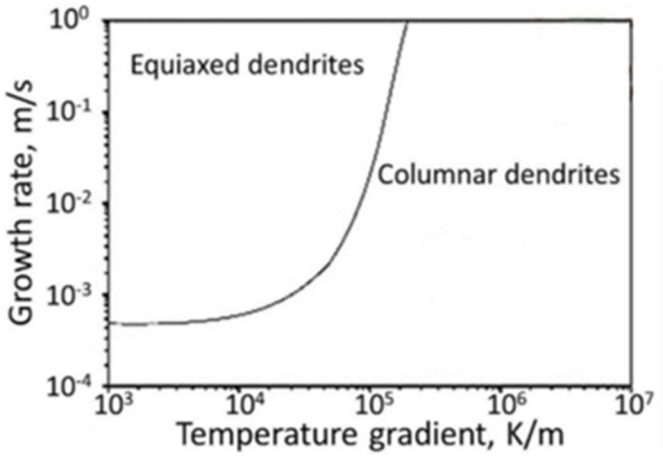

Figure 2: Transition from columnar to equiaxed grains based on G and R

4. Resultados

El análisis de los estudios publicados más relevantes hasta la fecha, representada en la *Figura 3*, indica que los valores de VED entre 65 y 100 J/mm³ son ideales para lograr muestras de muy alta densidad. Así mismo, rangos de VED específicos como 100 a 125 J/mm³ y 45 a 65 J/mm³, en diferentes estudios, revelan zonas donde la densidad óptima coexiste con defectos por “keyhole” y porosidad por “lack of fusion”. Los parámetros recomendados por este estudio para el sistema AconityMICRO incluyen un espesor de capa de polvo de 30 µm y

una distancia entre pasadas del láser de 0,080 mm. Esta selección de ajustes pretende que la ventana de fabricación óptima sea lo más amplia posible, consiguiendo alta densidad con mínimos defectos.

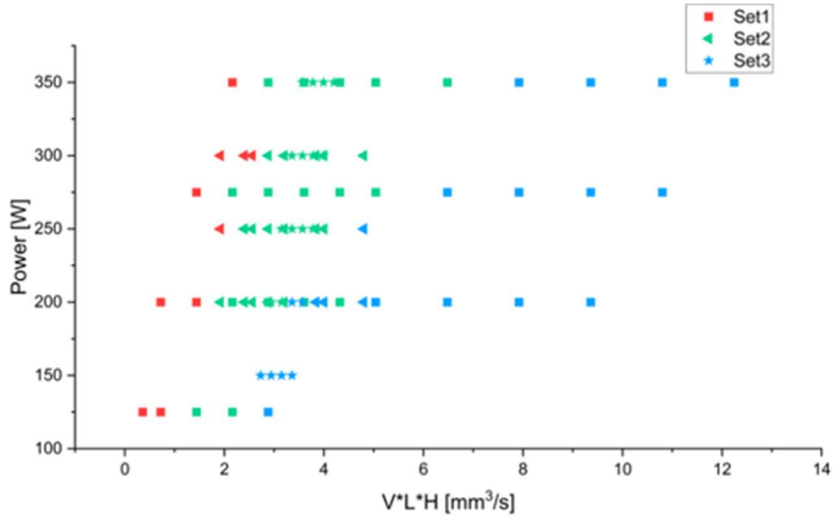

Figure 3: Plot of most relevant literature references

La formación y entrenamiento fueron componentes críticos de este proyecto. Los estudiantes de la Universidad de Cornell recibieron extensas sesiones de formación dirigidas por especialistas de la industria. Estas sesiones abarcaron la operación de la máquina, protocolos de seguridad, manipulación de interfaces digitales y el manejo seguro del polvo. Además, los estudiantes fueron instruidos en el uso de herramientas de software como Netfabb y Fusion 360 para diseñar y modelar piezas. También se practicaron técnicas de post-fabricación, incluyendo el pulido y la obtención de imágenes por microscopía para analizar futuras muestras fabricadas. Esta formación integral asegura que los estudiantes estén bien preparados para operar de manera independiente el sistema AconityMICRO y aplicar este conocimiento de manera efectiva y segura en futuras investigaciones.

5. Conclusiones

El estudio concluye con el cumplimiento de dos aspectos clave: El primero ha consistido en determinar un conjunto de parámetros de procesamiento críticos para lograr alta densidad en futuros trabajos en acero inoxidable 316L mediante la combinación de soluciones analíticas y estudios publicados previamente. Este marco basado en el enfoque de la densidad de energía volumétrica maximiza la ventana de fabricación óptima y predice la formación de defectos. Los rangos de VED establecidos proporcionan una sólida base para la predicción

de defectos y, en combinación con la predicción de la microestructura, ambos son cruciales para el éxito de las futuras construcciones en LPBF.

El segundo aspecto involucra los pasos necesarios para asegurar el correcto funcionamiento y manipulación de la máquina de LPBF en Cornell. Esto incluye la transmisión de información de los modelos CAD al software de la máquina y el dominio de los procedimientos de post-fabricación. Una futura evaluación de la precisión y aplicabilidad de los mapas de parámetros establecidos incluiría la creación y análisis de piezas para verificar el mapa de VED creado. El método propuesto incluye la producción de 15 muestras piloto, con parámetros distribuidos entre zonas óptimas, de transición y propensas a defectos. Este proceso de validación, combinado con sesiones de formación y técnicas de post-fabricación, asegura el correcto uso de la AconityMICRO por los ingenieros.

6. Referencias

[1] Oliveira, J. P., LaLonde, A. D., & Ma, J. (2020). Processing parameters in laser powder bed fusion metal additive manufacturing. Materials & Design, 193, 108762.

[2] Agrawal, A. K., Rankouhi, B., & Thoma, D. J. (2022). Predictive process mapping for laser powder bed fusion: A review of existing analytical solutions. Current Opinion in Solid State and Materials Science, 26(6), 101024.

[3] Yakout, M., Elbestawi, M. A., & Veldhuis, S. C. (2019). Density and mechanical properties in selective laser melting of invar 36 and stainless steel 316L. Journal of Materials Processing Technology, 266, 397-420

[4] Diaz Vallejo, N.; Lucas, C.; Ayers, N.; Graydon, K.; Hyer, H.;Sohn, Y. Process Optimization and Microstructure Analysis to Understand Laser Powder Bed Fusion of 316L Stainless Steel. Metals 2021,11, 832

Table of Contents

Chapter 1. Introduction 5

Chapter 2. Description of the technologies 7

2.1 AconityMICRO compact system by Aconity3D 7

2.2 Autodesk Netfabb and Fusion 360 Design Software 10

2.3 Characterization and Imaging resources 11

Chapter 3. State of the art 13

Chapter 4. Project Definition 17

4.1 Motivation 17

4.2 Objectives 18

4.3 Work Methodology and Planification 19

Chapter 5. Study of Density and Defects 21

5.1 Main types of Defects in LPBF Manufacturing 21

5.2 Volumetric Energy Density as a reference metric 25

5.3 Key Parameters and their Implications 26

5.3.1 Layer Thickness 28

5.3.2 Hatch Spacing 34

5.4 Implications of powder properties and size 36

Chapter 6. Grain Morphology and Size 39

6.1 Microstructural characteristics of LPBF manufactured metals 39

6.2 Morphology Plots: predicting microstructures 41

6.3 Analytical Approach: Rosenthal Equation 42

6.4 Expected morphology for 316L Stainless Steel 45

Chapter 7. Results 49

7.1 Definition of VED ranges for optimal builds 49

7.2 Microstructure characteristics expected upon research 54

7.3 Manipulating the AconityMICRO system 54

7.3.1 Training sessions by industry specialists 55

7.3.2 Netfabb and Fusion 360 ..... *56*

7.3.3 Post-processing practice *56*

Chapter 8. Conclusions and Future Work ***57***

Chapter 9. Bibliography ***59***

ANNEX I 65

ANNEX II 67

ANNEX III 68

Index of Figures

Figure 1: VED based processing map for 316L alloy [9]..... 11
Figure 2: Transition from columnar to equiaxed grains based on G and R..... 11
Figure 3: Plot of most relevant literature references 12
Figure 4: Additively manufactured orthopedic implant with lattice inner construction [1].. 6
Figure 5: AconityMICRO compact LPBF system [2]..... 7
Figure 6: Schematic representation of the laser powder bed fusion (LPBF) process [3]..... 8
Figure 7: Autodesk additive manufacturing software [4,5]..... 10
Figure 8: MULTIPREP™ 12" polishing station [6]..... 11
Figure 9: Olympus BX51 W1F electronic microscope [7] 11
Figure 10: Illustration of processing parameter influence on porosity [8] 14
Figure 11: Effect of temperature gradient (G) and solidification rate (R) on the developed microstructures [11]..... 15
Figure 12: Cross sectional images of parts containing (a) lack-of-fusion and gas porosity defects (b) balling (c) keyhole porosities [9]..... 25
Figure 13: Processing parameter map based on VED 28
Figure 14: Process parameters reported in the literature for producing SS 316L [24]..... 30
Figure 15: Effect of process parameters on porosity and defects sizes of 316L SS samples produced using (a) L35µm, (b) L50µm, and (c) L70µm [28]. 31
Figure 16: Optical microscope images of the polished surfaces of select samples built at different dwell times and powder layer thickness [27]..... 32
Figure 17: Defect percentage (porosity) and relative density for the samples printed with varying dwell times at different powder layer thicknesses [27] 33
Figure 18: Effect of layer thickness narrowing the optimal window for processing maps . 34
Figure 19: Relative density as a function of hatch distance shown by Nathalie et al. [24]. 36
Figure 20: Morphology associated to columnar grains [38]..... 40
Figure 21: Morphology associated with equiaxed grains [38] 41
Figure 22: Effect of temperature gradient G and growth rate R on the morphology and size of metallic microstructures upon solidification [42] 42

Figure 23: Thermal properties of 316L stainless steel 43
Figure 24: CET in a R vs G plot 45
Figure 25: G vs R solidification map [48] 47
Figure 26: Density of samples tested by Kamath el al. [34] 50
Figure 27: VED processing map results of Yakout et al. [24] 51
Figure 28: Optical micrographs from the cross-sections as function of P and V [25] 52
Figure 29: Plotting of most relevant literature references 53
Figure 30: Practice build during training 55
Figure 31: Selection of parameters for 15 sample testing 58

Chapter 1. INTRODUCTION

Additive manufacturing (AM), commonly known as three-dimensional (3D) printing has surged in popularity in recent years due to its remarkable versatility in design and its capacity to produce highly customizable parts and components from a 3D model. This increased popularity has been particularly evident in metal fabrication, where AM has proved its ability to produce structures with a high degree of geometrical complexity and performance in an efficient manner, whilst reducing time, costs and minimizing material waste. This capability has expanded the possibilities in component design, awakening special interest in industries such as energy, defense, and aerospace, where such resulting components were previously unattainable through traditional manufacturing methods.

Various techniques such as selective laser melting (SLM), directed energy deposition (DED), and electron beam melting (EBM) are included withing the metal AM scope. These methods share a fundamental principle: the deposition and melting of materials layer by layer using high-energy sources like lasers or electron beams. However, among these techniques, SLM, also commonly referred as Laser Powder Bed Fusion (LPBF), has emerged as an especially promising method, and will be the focus of this project.

In LPBF, powder feedstock is spread over as a powder bed layer and selectively melted by a heat laser source to build a component layer by layer. By repetition of these steps, intricate and reliable geometries such as lattice like structures become relatively simple to create, as shown in *Figure 1*.

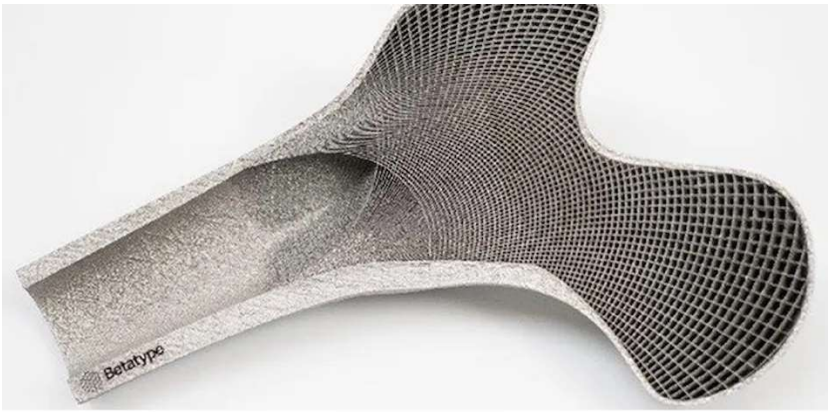

Figure 4: Additively manufactured orthopedic implant with lattice inner construction [1]

However, like any manufacturing process, LPBF is not without its challenges. Parts produced through this method often exhibit processing defects such as porosity, inclusions, and residual stress. The severity of these defects is influenced by the numerous processing parameters LPBF is based on, including laser power, scanning speed, hatch spacing, and layer thickness among the most relevant. Thus, to fully harness the potential of fabrication through LPBF, it is essential to have a sound understanding about how a part will be affected by its process parameters selection. Careful selection of an optimal processing parameter set is a deciding factor in whether a part meets its performance and quality requirements.

Chapter 2. DESCRIPTION OF THE TECHNOLOGIES

This chapter provides a detailed overview of the technologies and specific tools that support this project. These components and software are crucial to the project's development to a point it would not be coherent nor sustained without them. Therefore, their comprehensive description will facilitate the reader's understanding of the subsequent sections.

2.1 ACONITYMICRO COMPACT SYSTEM BY ACONITY3D

The vital piece of equipment that justifies this project is the *AconityMICRO* LPBF machine shown in *Figure 2*, located at the Grumman Laboratory within Cornell University. This resource, provided by the company Aconity3D, will be accessible at the academic institution upon its installation and authorization for safe operation; after training sessions are conducted to ensure the use of the machine is both effective and safe.

Figure 5: AconityMICRO compact LPBF system [2]

Before delving into the specifics of this compact LPBF system by Aconity3D, it is essential to explain the general operation of an LPBF machine. To facilitate understanding, an illustration of this type of additive manufacturing system is provided below in *Figure 3*, with its main parts and components labeled.

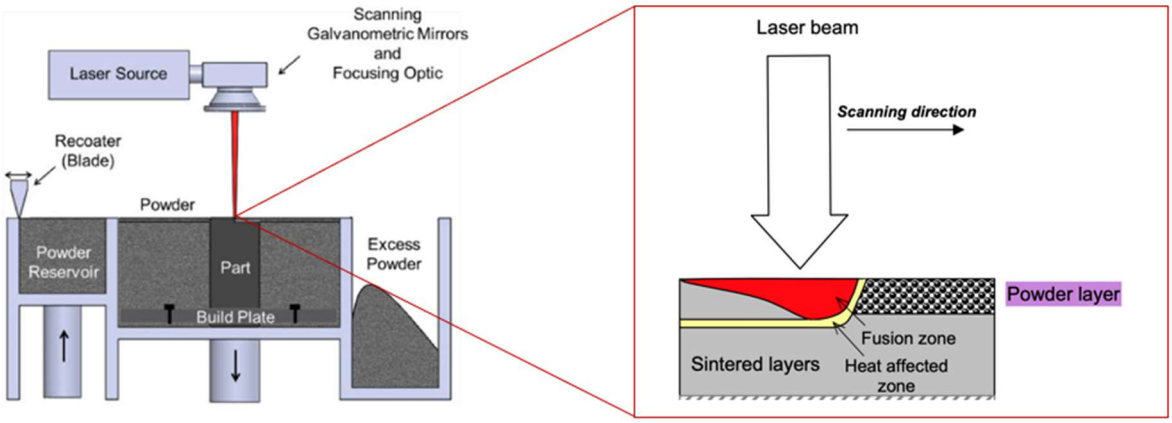

Figure 6: Schematic representation of the laser powder bed fusion (LPBF) process [3]

The common steps of a cycle of any LPBF machine consists of the following:

Once the powder supply cylinder is filled with the appropriate powder material, the build plate is lowered slightly from the recoater blade, and the build chamber is filled with an inert gas (usually Argon) to prevent oxidation during the whole process; all the preparatory steps are covered, and the machine is ready to initialize the build process.

Firstly, the powder deposition takes place, when the recoater blade spreads a thin layer of material across the build platform, ensuring an even distribution. Directed by the scanner system, the laser selectively fuses the powder in precise locations (which solidifies upon cooling to form a layer) based on the digital CAD model of the part that is being built.

Once a layer is completed, the build platform is lowered by a predefined layer thickness (usually around 20 to 100 µm [2]) and the recoater spreads a new layer of powder. Followed by another laser rescan, this process repeats, building the part from the bottom up as each new layer fuses to the previously solidified layer below it.

The post-processing steps upon completion and cool down of the part consist of raising the build plate to allow the removal of the piece from the platform. Excess powder is brushed or blown off and can be recycled for future builds. After being cleaned off, the finished part may undergo any necessary post-processing treatments such us machining, surface finishing or heat treatment among others.

The AconityMICRO, as every other LPBF machine, operates following these described steps. However, some more specific characteristics of this concrete device are the following [2] :

- An exceptionally fine laser spot size of 40 µm, which allows for high-resolution builds and intricate detailing. Paired with ability to spread very fine powders in layer thicknesses of less than 10 µm due to Aconity3D's revolutionary vibrating powder deposition, the surface finish and detail of the printed parts is significantly enhanced.
- AconityMICRO features a compact design making it suitable for spaced-constrained settings, and relatively easy to relocate within a facility, considering its weight of 850 kg. The downside to this portability is that only small to medium-sized parts can be built in its 100 mm diameter and 150 mm height build plate.
- The AconityMICRO is equipped with advanced monitoring systems that provide real-time feedback on the build process. This includes cameras and sensors that track the build environment and laser parameters. Furthermore, the machine employs closed-loop control systems to ensure consistent quality and precision throughout the build. Despite these advanced control systems, the machine operates on a very user-friendly web-based software, AconitySTUDIO, that simplifies the preparation and execution of print jobs, and even allows for remote machine access, which further contributes to flexibility in managing the build process.

- This device supports a wide variety of powder materials, including metals and alloys, which expands its versatility for different applications. This flexible material usage is paired with an effective powder handling design. It is equipped with completely extractable powder cylinders and a built tray which enable end-users to perform a very fast material change and quick start of the process, while ensuring recycling of unused or excess powder for future builds.

2.2 AUTODESK NETFABB AND FUSION 360 DESIGN SOFTWARE

Cornell University also grants the licenses required for operating both Netfabb [4] and Fusion 360 [5] software from Autodesk, which are indispensable digital tools to design the parts to be built by the *AconityMICRO* LPBF machine. These two CAD platforms allow for detailed modeling of parts that can be adapted and optimized to any specific requirements. Through these software interfaces, users can define key parameters such as layer thickness, support structures or material properties. All the information in these files is then seamlessly transferred to *AconitySTUDIO* [2], the operating software of the *AconityMICRO* system, where the manufacturing process is meticulously controlled and executed. This harmonized process ensures that the high precision and complexity that can be achieved in Netfabb and Fusion 360 are effectively translated into the final delivered part.

Figure 7: Autodesk additive manufacturing software [4,5]

2.3 CHARACTERIZATION AND IMAGING RESOURCES

One of the last crucial steps present in all scientific research regarding LPBF manufacturing is to conduct characterization and analysis (in our case, imaging) of the fabricated samples, in order to determine if the findings obtained correspond with the expected results. To perform this phase, Cornell University provides its research team with access to the MULTIPREP™ 12" [6] precision polishing system and the Olympus BX51 W1F [7] electronic microscope, both located at the Duffield Hall Laboratory. This facility is vital to achieve a precise assessment and examination of any samples that may be fabricated to test the influence of parameters and design choices in the outcome of the components.

Figure 8: MULTIPREP™ 12" polishing station [6]

Figure 9: Olympus BX51 W1F electronic microscope [7]

Chapter 3. STATE OF THE ART

Despite being a relatively new fabrication method, LPBF additive manufacturing has seen significant advancements in recent years, driven by a combination of technological innovation, materials development, and process optimization. Researchers have focused their efforts on the analysis of the microstructure, defects, surface finish and residual stresses of the manufactured parts. Various process variables have been considered in their studies, including laser beam properties, scan strategy, layer thickness, build orientation, as well as particle and powder properties.

Fabricating a defect-free, fully dense component in LPBF can be a major challenge. As a result, pore characterization and how to minimize defect formation during AM processing has been one of the primary goals. The volumetric energy density (VED) has been used as an approach to simplify the numerous LPBF parameters, and combining the most influential of them in an attempt to model the total energy input per unit volume that is delivered to the manufactured part [9].

This metric has been widely adopted as the guideline to determine whether a manufactured component through LPFB will be fully dense or, on the contrary, will present porosities and defects [8]. In LPBF, these might occur under two completely different conditions: insufficient VED yields to lack of fusion (LOF) defects, whilst and excessive value of VED leads to porosity that can be attributed to the occurrence of keyhole mode. Other characteristic defects include balling or gas porosity. Nevertheless, using both empirical and modeling techniques, researchers have proposed optimal ranges for VED, specific to each material and processing conditions, that result into high-quality dense parts. Results are commonly plotted in the form of VED based defect processing maps as *Figure 7*.

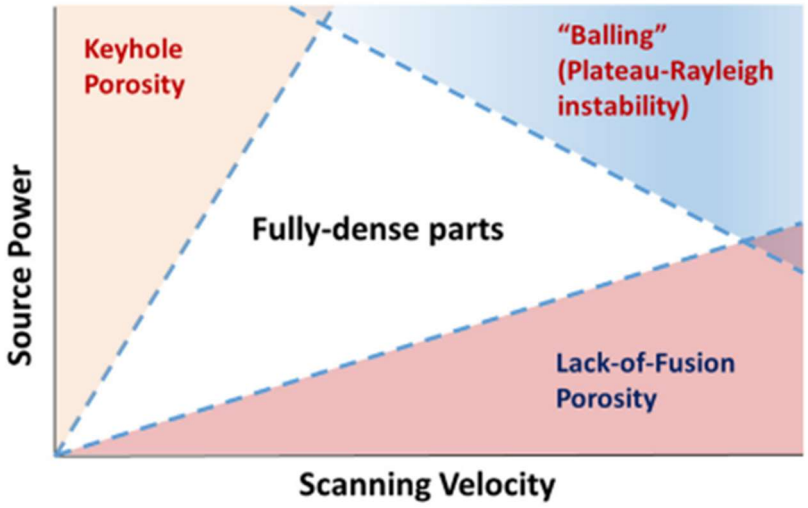

Figure 10: Illustration of processing parameter influence on porosity [8]

Another challenge in the LPBF process is the ability to predict and control the microstructure. Solidification microstructures are considered complex because of the moving laser heat source that overlaps with existing fusion tracks [10]. In addition, the moving heat source thermally affects layers that were previously formed as a function of spatial and temporal processing conditions. To better understand this phenomenon, a fundamental knowledge from welding metallurgy can be used, more specifically, an analytical method first introduced by Rosenthal [11] for a moving point heat source has been widely adopted in LPBF as to estimate the temperature field and melt pool dimensions. The microstructure has been found to be mainly dependent on the melt pool size and solidification conditions [10]: thermal gradient (G) and solidification rate (R) that can be derived from the Rosenthal equation. Recent studies have analyzed the morphology of the solidification structure (G/R) as well as its size (G*R), mapping these results for different materials as in *Figure 8*, where grain size and type can be predicted.

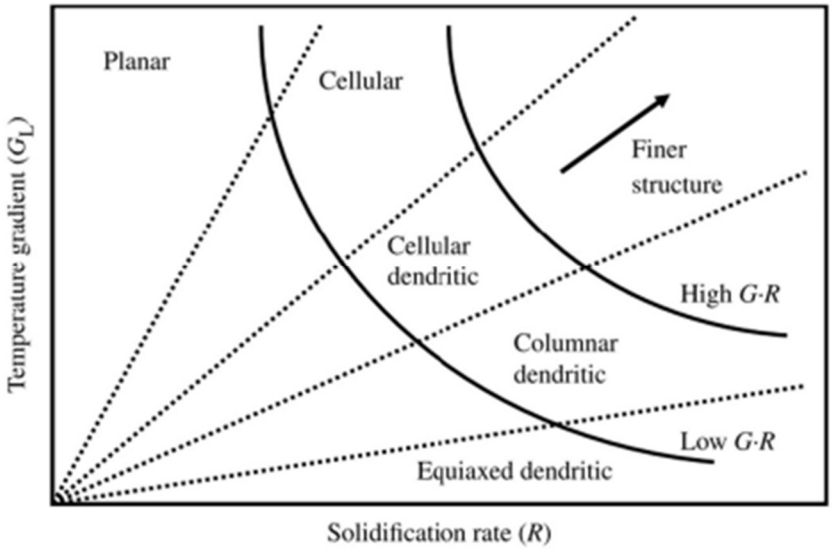

Figure 11: Effect of temperature gradient (G) and solidification rate (R) on the developed microstructures [11].

Regarding the material development in metal-based AM, several commercial alloys have been successfully used to manufacture engineering components by LPBF, including those based on titanium, iron, aluminum, or nickel-based superalloys [12, 13]. The material compatibility range has expanded very significantly in the recent years for LPBF, and this versatility stands as a great advantage for manufactures, who can now produce parts with tailored material properties perfected for specific applications such as heat resistance or exceptional structural strength under the most demanding of environments.

Despite these innovations, austenitic stainless steels are still to this day, the most extensively used material in LPBF manufacturing due to several key advantages that make it well-suited for this process: high corrosion resistance under aggressive environments, ensuring long-term durability; high ductility [14], reducing the likelihood of cracking or fracture during the production of complex geometries; good weldability; elevated temperature resistance and stability [15]; biocompatibility, making it suitable for patient-specific parts in medical and biomedical applications [16]; and finally its readily availability and relatively lower cost, especially compared to other alloys when a balance between performance and affordability

is desired. All these factors translate into grades 304L and 316L stainless steel to be the most commonly process in LPBF systems, and its implications of the most studied in the field.

Finally, advances in powder metallurgy techniques have led to the production of high-quality powders with controlled particle size distributions, spherical morphology, and minimal contaminants [17]. Consistent powder quality stands as a crucial factor for achieving uniform melting and minimizing defects in LPBF-produced parts.

Chapter 4. PROJECT DEFINITION

4.1 MOTIVATION

Cornell University Department of Materials Science and Engineering, within the Sibley School Mechanical and Aerospace Engineering, purchased the AconityMICRO laser powder bed fusion system from Aconity3D as of February 2024. This event marked a pivotal moment for the university's research community, opening doors to cutting-edge advances and innovation in additive manufacturing. This newly acquired technology presents a multitude of opportunities to explore AM capabilities and investigate in various rapidly growing fields such as advanced material research, innovative design, pushing the boundaries of engineering design freedom; and many other real-world manufacturing challenges the industry is currently facing. The acquisition of an LPBF machine as such is not just a technological investment, but a door to shaping the next generation of manufacturing solutions.

Nonetheless, before embarking on cutting-edge research using the recently acquired LPBF machine, it is vital to establish a comprehensive understanding of the fundamental principles underlying this manufacturing technique. Specially, given the lack of prior experience within the department at Cornell University regarding LPBF, it becomes crucial to develop a meticulously curated set of optimal processing parameters. This parameter set must ensure the production of high-quality, fully dense, defect-free samples within the specified range of operation, as well as portray the expected grain morphology/size. The need of establishing this solid reference framework (in the form of parameters and grain maps) is imperative before delving into unexplored research domains.

4.2 OBJECTIVES

The ultimate intention behind this project is to provide a solid framework that can serve as a reference point and ensure the validity and reliability of any new scientific endeavors carried out with the LPBF machine by the department at Cornell University. The specific goals are listed and explained below:

First and most important, developing a coherent and curated parameter set that minimizes part defects, involving a thorough examination of the extensive literature relative to analogous LPBF processes. This examination includes experimental investigations conducted by various researchers, analytical solutions derived from relevant equations, and predictive models also presented in published works. In addition, it is essential that these parameter sets are tailored specifically to the type of powder acquired by Cornell for use with the AconityMICRO machine, serving as a robust foundation for any subsequent scientific investigations conducted using the equipment. Parameter-specific maps based on the VED and other pertinent metrics must show the relationship between power and scan speed. With each chosen parameter set, this approach's objective is to produce an in-depth understanding of the expected results.

The second goal is to provide a basic understanding of the characteristic microstructures of additively manufactured 316L stainless steel through LPBF processes, including analytical methods and their correspondent experimental validations, that allow to predict the size and morphology of the grain structures. Since microstructure development dictates the final mechanical properties and performance of parts, through the appearance of phenomena as anisotropy; a sensible understanding of this topic is critical for engineers.

There are three parallel and crucial steps to succeed with the mentioned objectives and assure their future effective application: first, acquiring a thorough understanding of the machine itself including its manipulation and operation (the conduction of a training program on the AconityMICRO system by an industry professional provided by the machine's manufacturer is imperative); secondly, mastering the use of Netfabb and Fusion 360 software, which are

essential for transmitting part parameters to the LPBF machine and creating the desired components design. Lastly, upon the future manufacturing and testing of the selected parts (following the conclusions, results and recommendation of this project), it is necessary to conduct a comprehensive characterization process of said samples. This step involves polishing the parts and conducting an evaluation using electronic microscopy to analyze the results and compare them against the expected outcomes from the parameter map. This evaluation should specifically focus on addressing porosity defects and their impact on overall density, as well as imaging and an in-depth analysis of the primary grain characteristics. A key aspect to achieve this goal by a future team that follows this project is to ensure good understanding on how to operate the grinding and polishing stations available at Cornell Laboratories.

4.3 WORK METHODOLOGY AND PLANIFICATION

The proposed work methodology for this project combines a deep literature review and analysis of published works and experimental evaluations, in order to establish a solid preliminary framework that enables users of the AconityMICRO to manufacture 316L stainless steel parts with high density. The specific timeline for these activities is outlined below:

At the onset of the second semester: The project commences with a familiarization phase on the fundamental principles of LPBF AM. The focus will be put in a thorough exploration of each parameter's significance within this manufacturing method, paying special attention to the respective implications and effects of said parameters on the fabricated parts. An extensive literature review and analysis of published works will be conducted to create a coherent parameter-set map correlating Laser Power and Scanning speed variables. This will serve as the framework guiding our experimentation, and their results will be the foundation of future part production that may be undertaken to validate this project's conclusions.

From mid-February to mid-March: Since the installation of the AconityMICRO at Cornell Facilities will not take place until mid-March, work on a set of 25 316L stainless steel

samples will be done meanwhile. These samples, designed under a specific parameter choice, were manufactured by Aconity3D by the AconityMIDI machine, with the purpose of: firstly, gain insights into the type of results that could be expected from subsequent builds (given the fact that at said time Cornell does not have the capability to make their own samples); and secondly, take advantage of this timeframe to familiarize with the polishing station and grinding techniques essential for future sample processing.

In late March and the beginning of April: the project will focus on machine training sessions aimed at familiarizing the Cornell team with all aspects related to machine operation, powder manipulation, and the respective lab safety protocols. In addition to this, attention will also shift towards familiarizing with Netfabb software. Following the training session, the Cornell teams will engage in making a series of their own parts. This will serve as a validation of the skills acquired during this time. Additionally, as part of safety measures required by the department, a safety report and Standard Operating Procedures (SOP) will be submitted to Cornell authorities.

In late April and throughout the remaining month of May: All the knowledge, techniques and resources acquired during the semester will be combined and summarized in a final report that will serve as a framework and guidance on processing parameters and manipulation of the AconityMICRO at Cornell. Results will be evaluated and discussed.

Chapter 5. STUDY OF DENSITY AND DEFECTS

This chapter explores the challenges associated with maintaining density during the manufacturing of components using LPBF. If work operation takes place out of the known as optimal operating window (arrange of parameter values or ranges that result into nearly fully dense builds, synonyms of notable high quality), the LPBF process can be compromised by various types of defects such as excessive heat input, insufficient melting, or other forms of porosity, which can significantly impact the quality of the manufactured parts. As mentioned previously; in order to mitigate all of these issues, it is crucial to select a carefully curated set of parameters. In this context, this chapter provides an in-depth analysis of numerous published works and literature on said topic to draw conclusions about the implications of the different parameters and identify the optimal ranges that result into the most favorable results when manufacturing any 316L stainless steel part with the AconityMICRO.

5.1 MAIN TYPES OF DEFECTS IN LPBF MANUFACTURING

In general, during the fabrication of a part, defects can be created or transferred to the finished component in three ways [18], each of which correspond to subsequent stages of the LPBF manufacturing process:

1. Direct transfer from the feedstock powder: referring to imperfections or inconsistencies already present in the raw material itself used in the AM process, before any laser interaction occurs. The most common defects included in this category would be powder contamination by external particles, irregular powder shape and size, resulting into uneven melting and porosity; or surface oxidation in case of unproper handling or storage of the powdered materials.

2. Laser-Powder-Metal interaction during the melting stage: this is a critical step in the process where many defects may form depending on how well the powder particles melt and fuse together. Melt pool conditions far from the optimal could result into various kinds of defects such as insufficient or incomplete melting of the powder; on the contrary, and excessive heat input in the material, leading to deep, narrow cavities; the ejection of molten material, known as spattering; or excessively rapid heating and cooling rates that can induce thermal stresses, potentially leading to the appearance of cracks in the part.

3. Post-processing treatments: the final steps taken after the part has been built to improve its properties or prepare it for its final application can also introduce defects if not carefully controlled, most commonly residual stresses derived from fluctuating heat treatments; surface roughness, if material is removed unevenly during machining; direct contamination with external substances used during post-processing (oils, coolants, etc.); or imperfections due to incomplete removal of the part's supports.

In order to maximize density within any metal AM builds, all three mechanisms of defect transfer must be considered and thoroughly controlled. However, out of all of these, the laser-powder-metal interaction is the most common mean of porosity transfer in LPBF [18] and can be highly mitigated by the appropriate choice of processing parameters, thus it will be the focus of this study.

Among the defects that can appear due to the laser-powder-metal interaction, there are four main types commonly observed in LPBF [9,18] are lack of fusion (LOF) porosity, keyhole porosity, balling, and gas porosity.

1. LOF porosity [8, 19]: it occurs when the laser energy input to the powder layer is insufficient to fully melt the particles. This low transmission of energy results in incomplete bonding between layers or particles, and therefore leaving gaps or pores, which are often irregular in shape and are located at the boundaries of melt tracks, in

addition to weak mechanical properties due to said poor inter-layer adhesion. A large number of machine-controlled parameters have a direct effect on the presence of LOF porosity, however the most common causes are known to be: a sufficiently low laser power unable to melt the powder completely, an excessively high scan speed that does not permit sufficient time for adequate melting, a powder layer excessively thick so that the laser may not penetrate adequately to melt all particles; and lastly, a hatch spacing is too large as that there will be insufficient overlap of successive laser scans.

2. Keyhole porosity [8, 19, 20, 21] : a deep and narrow cavity (known as keyhole) in the melt pool is generated by an excessive energy input into the powder layer that is being processed, either caused by an overly high laser power or a too low scan speed. The pressure gradients and surfaced tension within the melt pool are translated into instability and fluctuations of the depth and with of the keyhole cavity, which is filled with metal vapor and other gasses due to the intense energy input. As the laser follows its build path, the keyhole rapidly collapses, and the gases can be trapped within the molten material, forming bubbles that become pores upon solidification. Often these pores are nearly spherical in shape due to the surface tension of the molten material and their distribution deeper in the material is most pronounced. However, irregular shapes are not discarded since keyhole dynamics can be erratic and complex and elongated pore shapes can as well be found. In order to prevent this typical form of defects in LPBF manufacturing, adjusting both the laser power and the scan speed to balance the energy input and avoid excessive melting is key.

3. Balling [8, 22]: this type of defects occurs when the formation of a stable and continuous melt pool as the laser passes is disrupted, and instead consecutive small spherical droplets constitute the printed track. The presence of these hump forms interferes with the continuity of the layers, resulting into an increased surface roughness and poor layer adhesion, potentially leading to structural integrity issues or dimensional inaccuracy of the part. The most common mechanisms that cause

balling are an insufficient energy input into the material, unable to fully melt the powder particles nor maintain a continuous melt track (however, the influencing factor in the balling phenomenon are extremely complicated and a high laser power paired with a high scan speed has also been found to promoted balling and an unstable melt pool); materials with an elevated surface tension (or large temperature gradients) when fused, becoming more likely to form spheres; an inadequate powder layering, due to poor spreadability and uneven distribution, or excessively thick powder layers; and an inappropriately large hatch spacing.

4. Gas porosity [23]: Despite this type of defect arising when gas becomes trapped within the melt pool and subsequently enclosed upon material solidification, similarly to keyhole porosity, it is considered a separated category, since gas is entrapped due to other mechanisms rather than the keyhole dynamics. These spherical gas pores are often caused by an inadequate inert gas flow that does not prevent the inclusion of atmospheric gases such as oxygen or nitrogen in the molten material; or an unstable melt pool influenced by fluctuating laser power or scan speed. Significantly reduced fatigue resistance and mechanical strength of parts (potentially leading to premature failure under loading), and a rough surface finish are some of the most appreciable effects on part performance caused by gas porosity.

These four types of defects (shown in electronic microscopy imaging in *Figure 9*) present in LPBF manufactured parts are difficult to eliminate via post-treatment methods such as heat and surface treatments, and among them, LOF and keyhole porosity are the most common and have the most adverse effects on the component's properties. Therefore, to ensure an appropriate quality and meet of requirements, as well as to reduce the market entry barriers of LPBF, a comprehensive understanding of the LOF and keyhole pore defects' formation mechanisms and their influence by the main processing parameters are imperative and are widely discussed in literature [20, 22]. Their prevention will be the focus of this study.

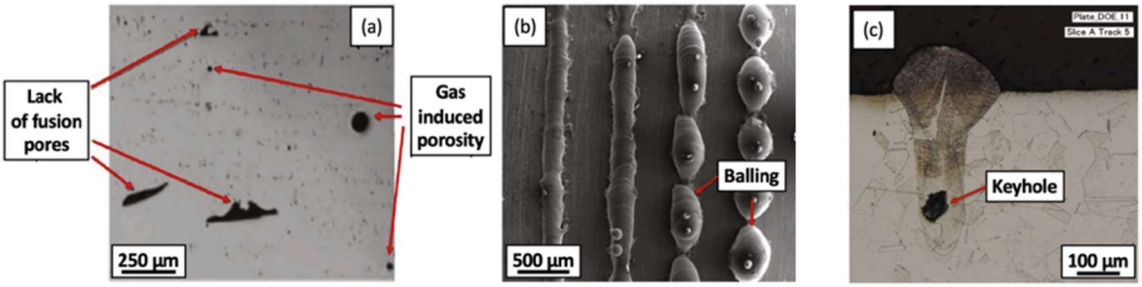

Figure 12: Cross sectional images of parts containing (a) lack-of-fusion and gas porosity defects (b) balling (c) keyhole porosities [9].

5.2 VOLUMETRIC ENERGY DENSITY AS A REFERENCE METRIC

The two most common porosity defects that affect the density of a part manufactured through LPBF that were previously discussed are both associated with the amount of direct energy input to the powdered material. In other words, an underdeveloped melt pool due to insufficient melting result in LOF, and on the contrary, excessive energy input produces keyhole dynamics. Consequently, an energy density-based metric that correlates the most influential processing parameters is necessary to predict these porosity phenomena [9] and classify them within real operating ranges of an LPBF machine.

The volumetric energy density (VED) has risen as the favored metric from this aspect, since it takes into consideration the four main processing parameters (laser power, scan speed, hatch spacing and layer thickness) that can each individually affect the properties of the manufactured product the most notoriously [24, 25]. This comprehensive measurement quantifies the total energy delivered to the material per unit volume (in J/mm^3), and engineers have established an empirical relationship to effectively predict and mitigate defects by adjusting the VED within optimal ranges.

$$Volumetric\ Energy\ Density\ (VED) = \frac{P}{V \cdot H \cdot L}$$

Equation 1

Where P is laser power (W), V is scanning speed (mm/s), H is hatch spacing (mm), and L is layer thickness (mm) [9]. VED has gained acceptance as a standard metric within the additive manufacturing community due to its ease of implementation and simplicity, whilst integrating critical process variables which if optimized can ensure consistent part quality. It is material-specific, with the ability to be empirically calibrated to optimize parameters for specific alloys and powders. Moreover, its widespread adoption by the research and manufacturing communities has resulted into the use of VED as reference in advanced simulation models, and experimental validation or standard of literature and published works. Considering all these factors, VED will be the guide to predict defects in this study.

5.3 KEY PARAMETERS AND THEIR IMPLICATIONS

As many other fully configurable LPBF systems, the AconityMICRO allows its user to adjust numerous processing parameters to a notably high degree. More specifically, the manufacturing process performed by this device can be optimized by configuring more than 200 different parameters [2]. This extensive range, whilst enabling very precise control over the production of high-quality, tailored parts; becomes unmanageable when it comes to optimizing such a large number of variables for a specific material and build. All considered, the four main parameters that constitute the VED expression (laser power, scan speed, layer thickness and hatch spacing) will be the ones this study seeks its optimization, for simplicity and relevance reasons.

It is important to note that many other parameters can highly influence the properties of the final part and the building process itself, such as the scanning pattern and overlap, the powder spreading speed, the inert gas flow rate or the preheating of the build platform among others [8, 9, 10]. However, as previously stated, for the sake of simplicity they will be kept fixed during this study to the recommended values by the machine manufacturer.

The amount of energy transferred to the powder layer (typically measured in Watts) is defined by the parameter known as laser power. It directly impacts the melting efficiency (described as of appropriate when there is a coherent fusion between successive layers;

excessive or unstable when keyholing occurs; or insufficient when LOF defects take place), as well as melt pool dynamics (higher laser powers increase the depth of the melt pool and the overlap between consecutive scan tracks). Other secondarily implications of the optimization of values of laser power that have been studied are thermal gradients and stresses, or surface quality [26]. It is crucial to note that in this study, the laser power will not be fixed to a concrete value, instead the available range dictated by the machine capabilities (up to 400 W in the case of the AconityMICRO [2]) will be explored and balanced with the other variable parameters in the VED equation, seeking for the optimal processing window.

Out of the four main parameters considered, the second one that will not be fixed to a specific value, but instead will vary along a range that optimizes the overall energy input, will be the scan speed. It is defined as the rate at which the laser spot moves across the powder bed during each layer fusion (typically measured in mm/s). The AconityMICRO offers a variable scan speed that can be configured up to 12.000 mm/s [2], providing a sufficiently broad range, especially considering the maximum laser power of 400 W. If other parameters are properly set, LOF defects are likely to occur well before reaching the maximum scan speed, and consequently, this parameter will not be the limiting factor in the process.

The objective behind varying these two parameters unrestrictedly is the creation of a VED-based map where the coordinate axis are scan speed and laser power. This plot would be separated in different areas whose boundary lines depend on the VED ranges and are associated on the one hand to tendency or likelihood of appearance of a particular type of defect, or on the contrary to an optimal window of high quality, defect-free parts [26] as shown in Figure.

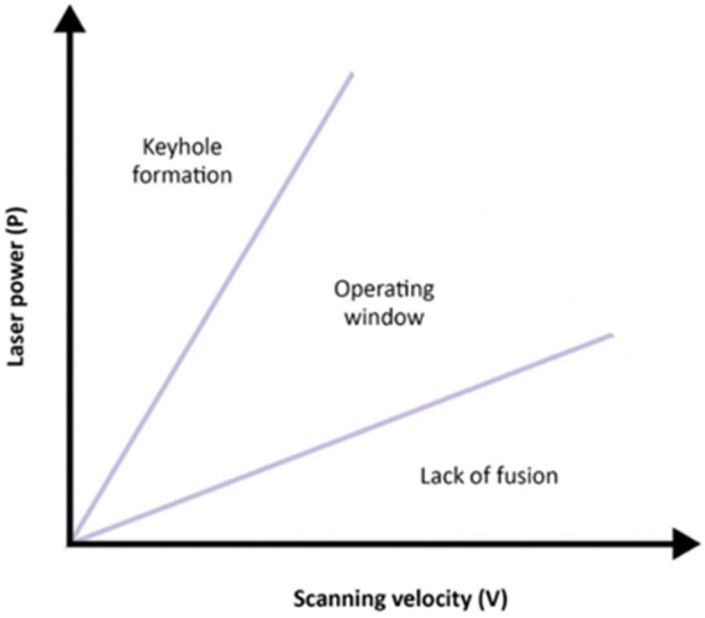

Figure 13: Processing parameter map based on VED

In order to build a processing map that illustrates the operating windows and defect boundaries with such simplicity and effectiveness, the remaining parameters that constitute the VED expression (layer thickness and hatch spacing) must be fixed to the values that are more likely to expand the optimal operating window to its largest, granting the most satisfactory results. Therefore, the following two subsections deeply analyze these parameters in order to find the most optimal values.

5.3.1 LAYER THICKNESS

In the context of LPBF manufacturing, layer thickness refers to the height of each individual layer of powder that is spread across the build platform by the recoater (fully covering the build plate) before it is selectively melted by the laser. This is a critical parameter from two different perspectives: layer thickness greatly influences the resolution, finish and overall quality and properties of the final part; while it is also a parameter that can be optimized to minimizing the build times and cost [27, 32, 33]. Unfortunately, both advantages cannot be achieved at the same time.

It is an obvious statement that thicker layers of powder significantly increase the build rates of any LPBF job, since the necessary time to process one individual layer, despite its thickness, is equal to another. At the same time, the total number of layers necessary to complete a build is equal to the total height of the manufactured part above the build plate divided by the layer thickness. Therefore, by increasing the layer thickness, a smaller number of layers are needed to achieve the total heigh of the final product, thus build time is directly minimized and efficiency rises. The following expression can be used to estimate the build rate of an LPBF job (in units of mm^3/s) [27]:

$$Build\ Rate = V \cdot L \cdot H$$

Equation 2

Where V is the scan speed, L is the powder layer thickness, and H is the hatch spacing. This expression does not factor in the powder fill and wiping time between each laser cycle, but it does provide a general idea of how variations in processing parameters affect the build rate.

Nevertheless, the process of selecting the appropriate layer height cannot only rely on efficiency optimization. Whilst thinner layers may slow down the manufacturing process, research has shown that they enable higher resolution and finer details, smoother surface finishes, as well as a higher part density and consequently improved mechanical properties [27, 28, 29].

The typical and sensible ranges of layer thickness for conventional LPBF builds using 316L stainless steel are between 20 and 100 µm (the millimeter is also a common unit used for this metric), where the higher sections (between 70 and 100 µm) are most suitable for faster production, partly sacrificing density and refinement, while the smaller ranges (between 20 to 40 µm) are focused on delivering high precision parts [32, 33].

The machine capabilities also dictate the possible ranges for layer thickness. In the case of the AconityMICRO, this parameter can be set between a broad range of 5 µm up to 100 µm

[2]. Since this span includes in the previously discussed and commonly used range for 316L stainless steel parts, the machine capability does not compromise this study.

The following table shown in Figure summarizes the LPBF processing parameters that have been reported in the literature for producing stainless steel 316L parts up to the year 2018, gathered by Yakout et al. [24].

Reference	*P*(W)	*v*(mm/s)	*t*(mm)	*h*(mm)	E_v(J/mm^3)
Stainless steel 316L					
Kamath et al. (2014)	150-400	500-1800	0.030	0.150	28-74
Li et al. (2012)	190	800	0.050	0.150	32
Miranda et al. (2016)	50-100	300-1250	0.030	0.070-0.140	32-80
Spierings et al. (2010), Spierings and Levy (2009)	104	175-800	0.030-0.045	0.130	33-107
Kruth et al. (2010b)	100	175-380	0.060	0.126	35-76
Yasa et al. (2009)	85-105	300	0.020-0.060	0.112-0.125	38-156
Yusuf et al. (2017)	200	1600	0.050	0.060	42
Liu et al. (2011)	50	100-300	0.050	0.080	42-125
Casati et al. (2016), Yakout et al. (2018a)	200	750	0.050	0.110	48
Kruth et al. (2010a)	105	380	0.020-0.040	0.125	55-111
Dadbakhsh et al. (2012)	87	150	0.075	0.130	59
Kurzynowski et al. (2018)	100-200	200-220	0.050	0.124	81-150
Yadroitsev and Smurov (2010)	50	120	0.040	0.120	87
Yasa et al. (2010)	100	300	0.030	0.081-0.126	88-137
Yasa (2011)	100	300	0.030	0.112-0.125	89-99
Sun et al. (2016)	380	625-3000	0.050	0.025-0.120	99-109
Liverani et al. (2017)	100-150	700	0.020	0.050-0.070	102-214
Saeidi (2016)	190	800	0.020	0.100	119
Yadroitsev and Yadroitsava (2015)	50	100	0.050	0.070	143
Liu et al. (2016)	200	400	0.040	0.080	156
Yadroitsava and Yadroitsev (2014)	50	100	0.050	0.060	167
Shifeng et al. (2014)	180	900	0.020	0.060	167
Yadroitsava and Yadroitsev (2015)	50	100	0.040	0.070	179

Figure 14: Process parameters reported in the literature for producing SS 316L [24]

Under the fourth column labeled as “t (mm)” the values used for layer thickness in units of millimeters are displayed. It can be clearly interpreted that the most commonly used layer height was of 30 to 40 µm, aiming for precise builds and prioritizing the mitigation of defects over build rate efficiency.

More recently published works, deeply analyze the implications of varying the layer thickness in additively manufactured stainless steel 316L:

Figure 12 shows the results of porosity variation depending on layer thickness encountered in 270 SS316L fabricated samples [28]. These were produced using three different layer heights of 35, 50 and 75 µm and maintaining a fixed hatch spacing of 120 µm.

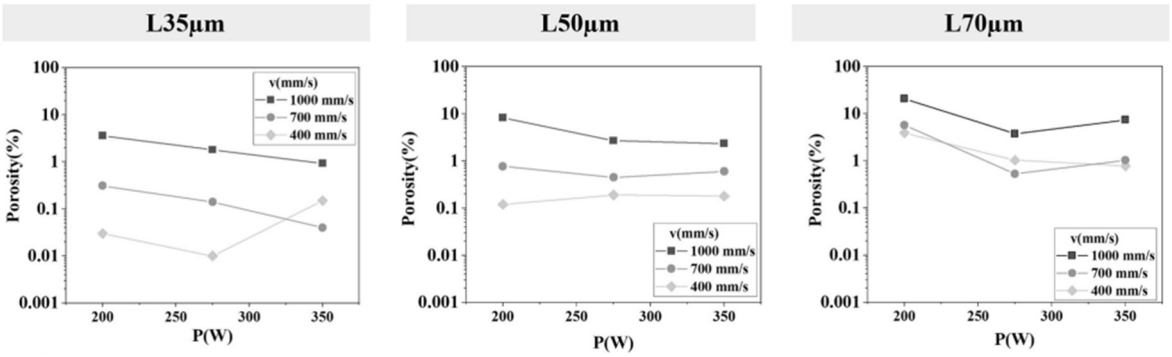

Figure 15: Effect of process parameters on porosity and defects sizes of 316L SS samples produced using (a) L35µm, (b) L50µm, and (c) L70µm [28].

It was reported that the samples produced with the thickest layer height of 70 µm had the highest porosity and largest defects within the applied range of linear energy (for equivalent values of power and scan speed). Furthermore, the layer thickness 35 µm (thinnest within the discussed optimal range) resulted in the lowest porosity as compared to 50 µm and 70 µm counterparts.

Additional studies by Yasa et al. [29, 30, 31] corroborated this just mentioned results, as they indicated that, for a fixed power and scan speed, under optimal values of VED for 316L stainless steel, the density improved as the layer thickness was reduced, with a layer thickness of 30 µm resulting in the highest density.

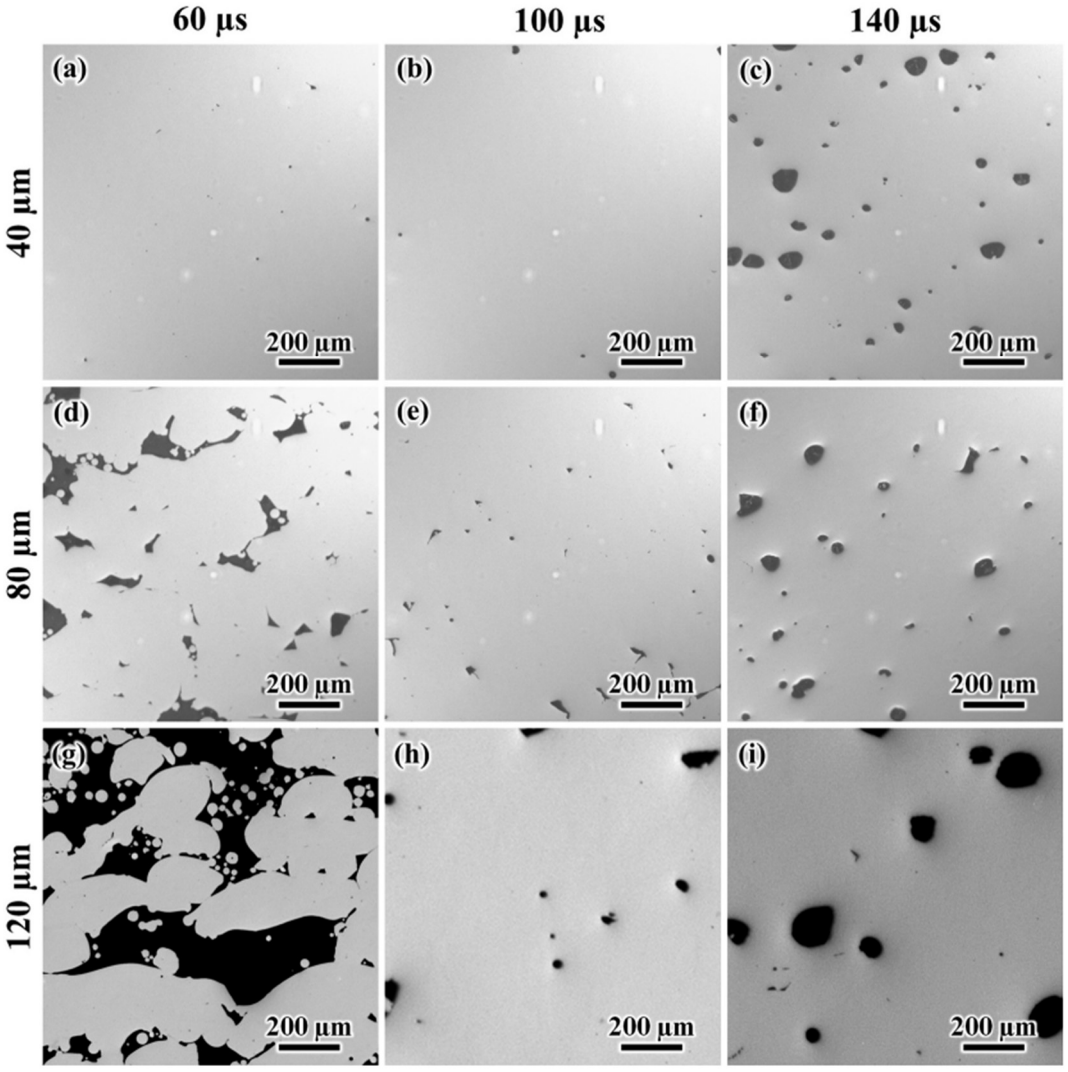

Figure 16: Optical microscope images of the polished surfaces of select samples built at different dwell times and powder layer thickness [27]

Another parallel recent study [27] on the effects of powder layer thickness on the microstructural development of AM SS316L. From the optical microscope images shown in *Figure 13*, the author concludes that for fixed values of the other VED parameters and an optimal range of dwell times (referring to the time the laser is activated and working on the powder, which is directly proportional to input of heat) the thinner layer thickness of 40 µm resulted into higher densities compared to the larger layer thicknesses. The results [27] of the different samples tested were summarized in the Figure 14:

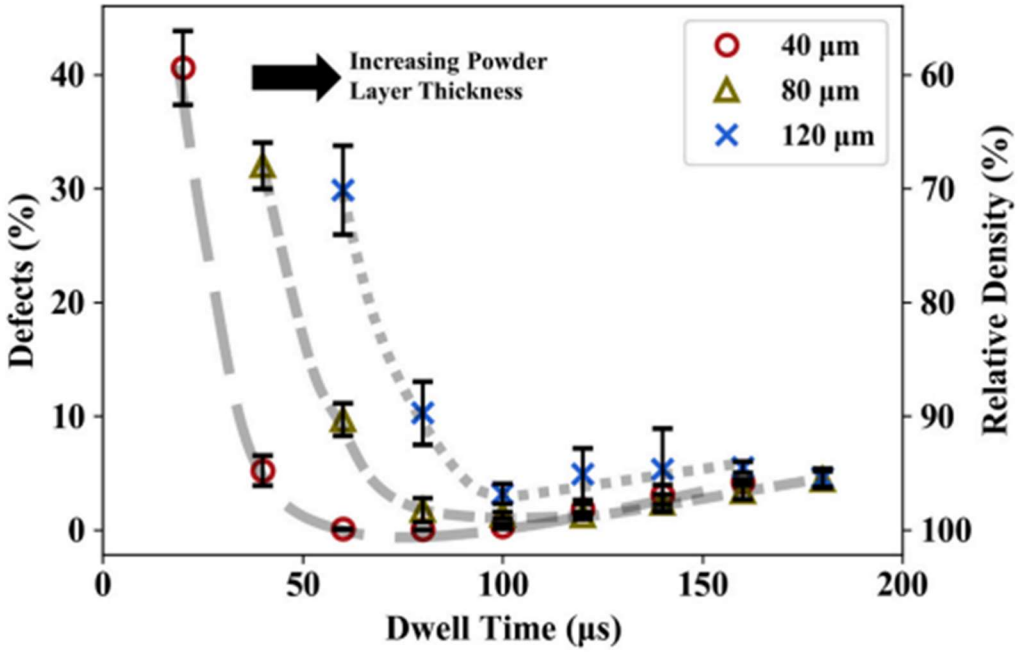

Figure 17: Defect percentage (porosity) and relative density for the samples printed with varying dwell times at different powder layer thicknesses [27]

After the analysis of the discussed published works, this study can conclude that thicker layers require deeper penetration of the laser energy to ensure complete fusion to the metal powder below. Therefore, for a fixed energy input, as the layer thickness increases the optimal operating window for any specific LPBF process narrows [28], as shown in *Figure 15*. Since build rates are not a concern of this study, and taken the published results, a thinner layer thickness between 30 and 40 µm will most likely deliver the largest optimal processing window in a VED map for SS316L builds.

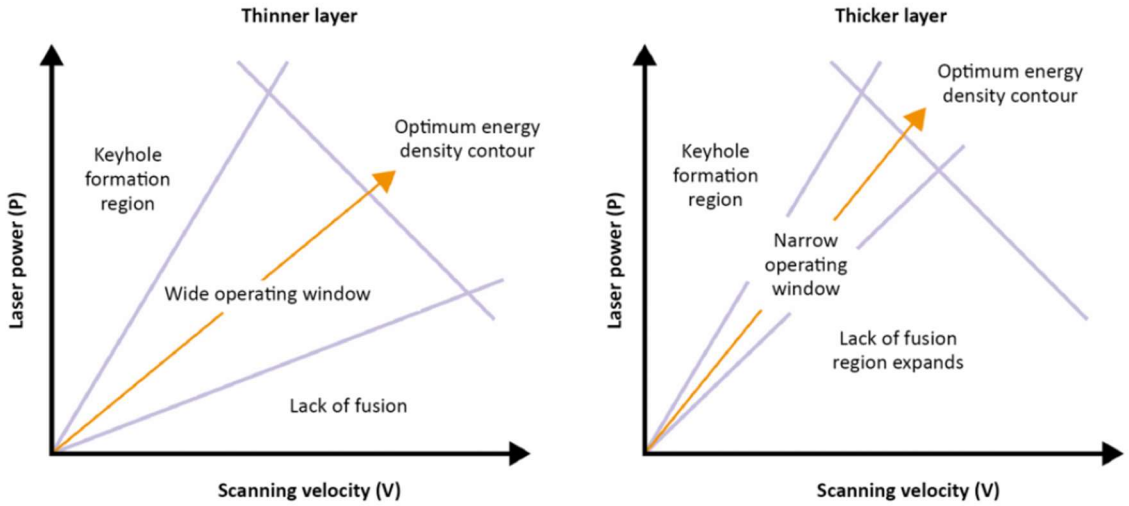

Figure 18: Effect of layer thickness narrowing the optimal window for processing maps

5.3.2 HATCH SPACING

The hatch spacing determines the amount of overlap between two adjacent laser tracks, as this parameter is the measured distance between two consecutive scan lines. It has a direct impact on defects and consequently overall quality of the fabricated part: an optimal overlap between laser passes tends to favor complete fusion and high part density. Meanwhile, an excessively large or too low of a hatch spacing may lead to insufficient melting (likelihood of LOF defects) or and excessive energy input (keyhole), respectively [35].

Similarly to layer thickness, hatch spacing is of great relevance to optimizing build rates (see *Equation 2*). Engineer may consider that smaller hatch spacing significantly increase build times due to the higher number of scan lines required, and a larger value for this parameter is likely the choice for prioritizing efficiency and cost saving [27].

For stainless steel 316L additively manufactured parts, a generally accepted and sensible range for hatch spacing is between 50 to 200 µm or 0,050 to 0,200 mm. If strong mechanical properties and low porosity are the priority requirements, the lower half of the range may be

the most suitable; whereas the higher half translates for faster builds where high density is not as critical.

Earlier work done by Kruth and Yasa et al. [30, 31] indicated that using 100 W laser power, a scan speed of 300 mm/s, layer thickness of 30 µm with a large spot size of 180 µm resulted in high-density stainless steel 316L parts, when using, and hatch spacing factor of 0.62. In other words, hatch spacing was set to the hatch spacing factor times the spot size. Given the large spot size of the machine used in the study and the setting of the hatch spacing factor, this resulted in a hatch spacing of 112 µm for optimal builds.

Similarly, another of their studies [29] on the same material showed highest density at fixed power of 105 W (with a slightly larger spot diameter of 200 µm), scan speed of 380 mm/s and a hatch spacing of 125 µm (applying the same factor as previously mentioned). These optimal values of hatch spacing are coherent with the common ones shown under the fifth column labeled as "h (mm)" in processing parameter table set by Yakout et al. [24] shown in *Figure 11*.

Nonetheless, since the spot diameter of the AconityMICRO machine is much smaller than the one used in this prior work, at 40 µm [2], these conclusions and relation between hatch spacing and an optimal hatch spacing factor of 0.62 cannot be directly applied. However, this prior research provides an estimate of the optimal parameter for layer thicknesses of 30 µm of stainless steel 316L. This estimate may be slightly minimized due to the smaller spot size of the machine this study is designed for.

A more recent published study [24] examined the effect of hatch spacing on LPBF stainless steel 316L manufactured parts under constant layer thickness, laser power and scan speed of 30 µm, 200 W, and 800 mm/s, respectively. Hatch spacing was varied between 0.08 mm, 0.1 mm, 0.12 mm, 0.14 mm, and 0.16 mm. The results are depicted in Figure. The general tendency as the hatch distance decreased, was an increase in density. However, the relative density remained mostly greater than 99.8%, even at large hatch distances of 0.16 mm, which is much larger the laser beam diameter used, the melt pools were sufficiently large, and they

overlap to minimize the LOF flaws. Conclusion could be made that the variation of hatch spacing does not have as of a detrimental effect on density as layer thickness.

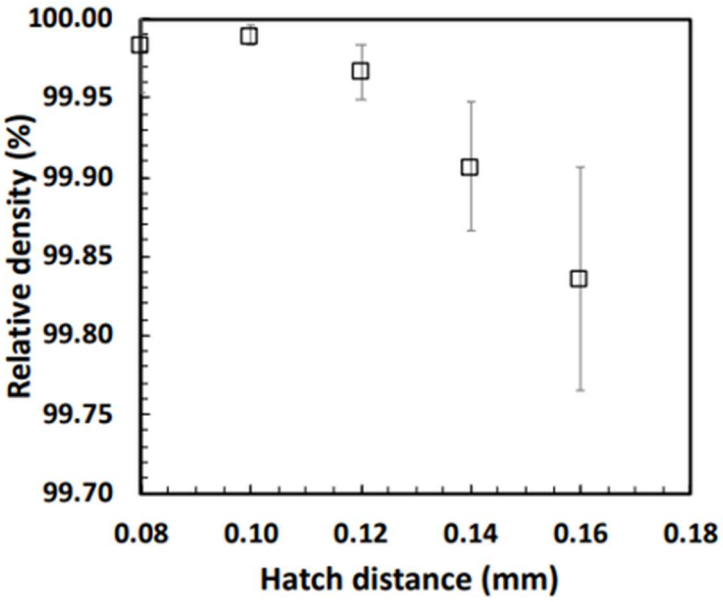

Figure 19: Relative density as a function of hatch distance shown by Nathalie et al. [24]

5.4 IMPLICATIONS OF POWDER PROPERTIES AND SIZE

A published study done by Ziri et al [28] showed how the properties of the powder used are crucial determinants of the quality and characteristics of the final product, thus the topic's relevance to this project is evident. The paper in question investigates the effects of different powder types and particle sizes on the porosity and overall quality of 316L stainless steel components produced through LPBF. The three stainless steel 316L powder types involved are:

I. A fine powder (Type1-H6) of mean diameter of 6 µm and particle size distribution (PSD or D90) below 18 µm.
II. Two standard powders (Type2-H27 and Type3-S34) of mean diameter of approximately 27 µm and 34 µm, respectively, along with a PSD (D90) below 60 µm.

III. A coarse powder (Type4-H67) of mean diameter of 67 µm and PSD (D90) above 50 µm.

The following conclusions were drawn:

1. PSD significantly impacts the homogeneity and density of the powder layer, which in turn affects defect formation. Whilst fine powders tend to have poor flowability and a high tendency for agglomeration which lead to an uneven or inhomogeneous layer deposition and higher porosity in the final parts; standard powders with a more balanced PSD contribute to more uniform layers, thus lower porosity. More specifically, the study found that fine powders had approximately 20% lower apparent density compared to their coarser counterparts.
2. The optimum VED varies with the PSD and powder properties. While standard powders were found to perform best within the VED range of 62.5 to 104.2 J/mm³ (as reported in the literature [24]), coarser powders (D50 = 73 µm) had a narrower optimal processing window therefore exhibiting higher porosity, mainly due to significant spattering during the build process. Fine powders, due to their insufficient flowability as previously mentioned, also required higher VED to achieve nearly dense parts but still showed higher porosity compared to standard powders.

In conclusion, the recommended powder type for producing 316L stainless steel parts are standard size powders since they have been proven to provide the best outcomes in terms of lower porosity and smaller defect sizes, due to their balanced PSD and better flowability. The 316L powder acquired by Cornell University to be used in future experiments with the AconityMICRO has a mean diameter (D50) of 31 µm, and D90 of 48 µm, considered standard powder so as to maximize the optimal processing window in future builds. The specification sheet and test certificate of the powder is included in Annex 3.

Chapter 6. GRAIN MORPHOLOGY AND SIZE

This chapter aims to furnish the reader with fundamental insights about the microstructure of stainless steel 316L parts fabricated via LPBF. Whilst a deep and comprehensive analysis of this complex topic may be beyond the scope of this study, only the essential details on the development of grain morphology and size in LPBF processes will be provided, along with the implications of these microstructural characteristics. An overview of analytical models and key studies from existing literature will also be discussed, as well as an evaluation on how these resources may equip the reader with a sensible understanding and the ability to predict the microstructures of parts produced using the AconityMICRO system.

6.1 MICROSTRUCTURAL CHARACTERISTICS OF LPBF MANUFACTURED METALS

Fusion-based metal additive manufacturing processes in general are featured by small melt pools and steep temperature gradients from the solid–liquid interface toward the liquid metal. During this process, solidification occurs in conditions that are far from equilibrium and possesses, in the majority of cases, a strong directionality [35, 36]. All factors considered, and added to the rapid melting and solidification rates inherent to the LPBF technique, the metallic materials including 316L stainless steel, exhibit unique morphologies. The microstructures are most characterized by columnar grains, with cellular tree-like dendritic structures; or in contrast the finer and smaller equiaxed grains, more exceptionally achieved [35, 37].

The first of the two types, the columnar grains, are elongated in from and oriented in the direction of the thermal gradient, typically along the build direction (perpendicular to the build platform). Their growth is at peak when the cooling rates are exceptionally rapid and the steeper the thermal gradients are [38]. *Figure 17* shows the morphology of columnar grains.

Figure 20: Morphology associated to columnar grains [38]

Depending on the application of the manufactured part, a columnar grain microstructure may not be the most advantageous from, since it incorporates anisotropic properties to the material. Anisotropy refers to the directional dependence of material properties, meaning that these vary based on the orientation of the material relative to the applied loads or stresses, thus compromising the physical behavior of the parts [39]. While tensile strength, fatigue and resistance to deformation along the grain growth direction may be enhanced, orthogonal strength (perpendicular to the grain growth direction) significantly weakens, since the grain boundaries act as planes of weakness where cracks may initiate and rapidly propagate. This behavior of some additively manufactured metals may be detrimental to component qualification or targeted applications under certain types of loading [40].

The microstructure could be also composed of equiaxed grains, which are finer than columnar grains and characterized by being approximately equal in all dimensions, therefore contributing to an isotropic microstructure [35, 36, 38]. Thus, solving the directionality differences in properties previously discussed. Equiaxed grains growth is enhanced by lower thermal gradients and a high nucleation rate. *Figure 18* shows the morphology of equiaxed grains.

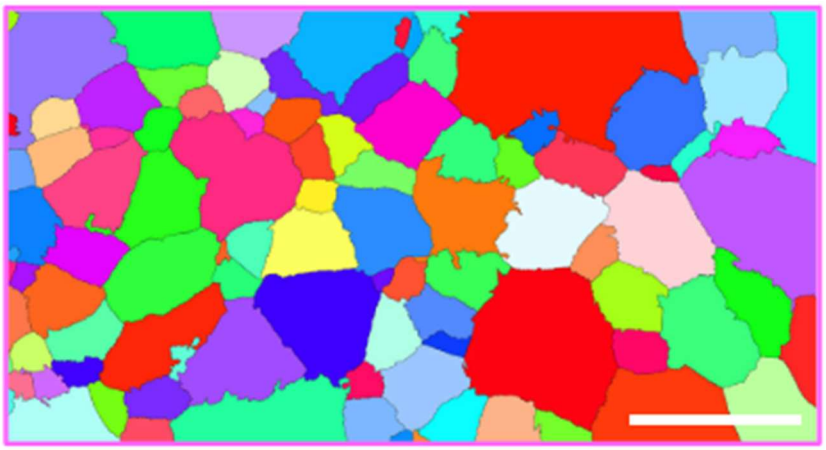

Figure 21: Morphology associated with equiaxed grains [38]

6.2 MORPHOLOGY PLOTS: PREDICTING MICROSTRUCTURES

In order to predict the type of microstructure and model solidification processes far from equilibrium, morphology plots are employed. It is well established in the scientific community that directional solidification can be effectively described and modeled through the use of two distinct solidification parameters [41, 35]:

I. The temperature gradient at the solid-liquid interface (G), which is commonly expressed in K/mm.
II. The growth rate of the solidifying front (R), frequently expressed in mm/s.

The direct and inverse relationships between these parameters are used to predict the resulting grain morphology and size for LPBF metal manufacturing, as follows:

I. The product between these two quantities (G·R), commonly expressed in units of [K/s], represents the cooling rate of the material within the solidification interval and therefore controls the size or scale of the resulting microstructural grains, with finer microstructures being achieved at higher cooling rates and coarser at lower G·R.
II. The ratio between the temperature gradient and the growth rate (G/R), frequently expressed units of [$K \cdot s \cdot mm^{-2}$], models the morphology of the solidified grains: as

G/R is decreased (thermal gradient (G) lowers, and solidification rate (R) increases), a transition from the columnar grains, to equiaxed is commonly observed.

Several published works have been devoted to the quantification of these solidification parameters in order to plot them and predict resulting microstructure of additively manufactured parts. *Figure 19* is an example of the aspect of a general plot that shows the effect of temperature gradient G and growth rate R on the morphology and size of metallic microstructures upon solidification.

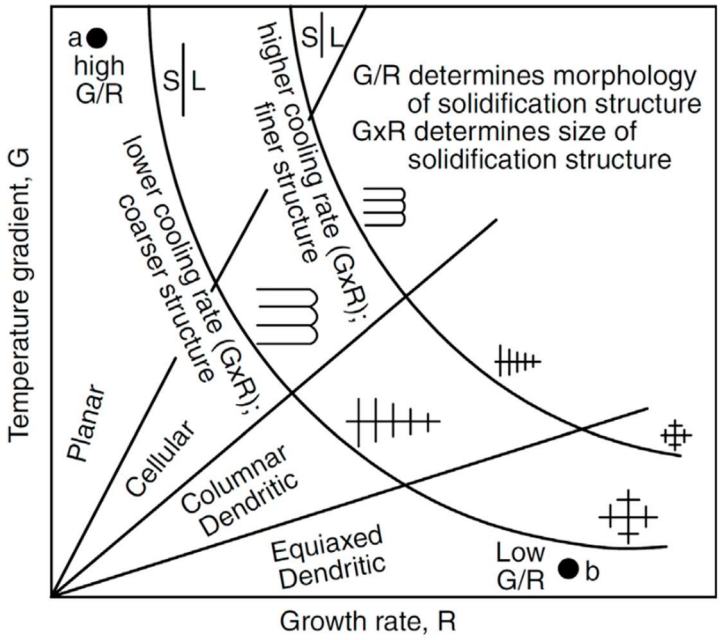

Figure 22: Effect of temperature gradient G and growth rate R on the morphology and size of metallic microstructures upon solidification [42]

6.3 ANALYTICAL APPROACH: ROSENTHAL EQUATION

To understand and predict the microstructure of 316L stainless steel components fabricated using the AconityMICRO, the user may face the necessity to relate the solidification parameters discussed in the previous section to the processing parameters that are responsible for the proper functioning of the machine and govern the manufacturing process. A simple, yet validated thermal model, originally developed for the welding industry and

first introduced by Rosenthal [11] can provide the needed quantitative relations in the context of LPBF. This analytical solution models the three-dimensional temperature field of a moving point heat source, thus the estimation of the melt pool dimensions and temperature distributions. The following simplified equation models the two-dimensional temperature field:

$$T(x,y) = To + \frac{Q}{2\pi kr}\exp\left(\frac{-vr - vx}{2\alpha}\right)$$

Equation 3

Where T_0 is the initial domain temperature, r is the distance from the laser point source ($r = \sqrt{x^2 + y^2}$), Q is the effective power input, defined as the laser power multiplied by absorptivity (taken as 0.35 [43]), v is the moving speed of the laser source along the x direction (scan speed), k is the thermal conductivity (and α is the thermal diffusivity, both calculated at the melting temperature [35]. The laser beam is scanning the substrate along the x direction, while y is directed orthogonally to the substrate surface.

The following table shown in Figure 20 includes the values for 316L stainless steel thermal properties by [44, 45]:

Property	Value	Units
Melting temperature (T_m)	1375	°C
Thermal conductivity (k)	29.5	W/mK
Density (ρ)	7318	kg/m^3
Thermal diffusivity (α)	0.05	cm^2/s

Figure 23: Thermal properties of 316L stainless steel

For the temperature map introduced by Rosenthal to be effective, it is necessary to consider the following assumptions: latent heat of solidification is neglected, as well as convective and radiative cooling into the surroundings (exclusively heat transfer via conduction). Fluid flow within the melted region is ignored (steady state) and thermal properties are assumed constant throughout the calculations [11,35].

The Equation can be easily programmed into a software like MATLAB to obtain the temperature fields along a layer of powder above the substrate plate as the laser inputs heat over the material. Once the temperature field is known (basing on the thermal properties of 316L stainless steel and the previously selected process parameters) the temperature gradient (G) can easily be calculated by vectorially adding the two components Gx and Gy as shown in *Equation 4* [35]:

$$G = \sqrt{{G_x}^2 + {G_y}^2}$$

Equation 4

Where the components can be calculated directly from the temperature field as:

$$G_{x,y} = \frac{dT_{x,y}}{dx\ dy}$$

Equation 5

Therefore, the first solidification parameter G has been directly related to the processing parameters present in the Rosenthal equation (laser power and scan speed). In the case of the solidification rate (R), it is known to be linked to the laser scan speed by means of *Equation 6* [35]:

$$R = v \cdot cos\beta$$

Equation 6

Where the angle β between the heat flow direction and the laser scanning direction has been calculated in previous literature by DebRoy et al. [46] as:

$$\beta = tan^{-1}\frac{G_y}{G_x}$$

Equation 7

6.4 EXPECTED MORPHOLOGY FOR 316L STAINLESS STEEL

This final section aims to provide a concrete understanding of the typical microstructures to be generally expected in 316L stainless steel parts manufactured through conventional LPBF processing. Basing on previous literature and published research, it will clarify the anticipated morphological characteristics depending on theoretical models, previously presented concepts and analytical solutions, contrasted with experimental data. These studies specifically address the 316L steel alloy of interest for this study on the AconityMICRO system.

Theory exposes that, as G/R decreases, the morphology of the grains shifts from columnar dendritic to equiaxed dendritic. The key idea is that when the ratio of G to R falls below a certain critical value, equiaxed grains are more likely to form, leading to the columnar-to-equiaxed-transition (CET) [35] .

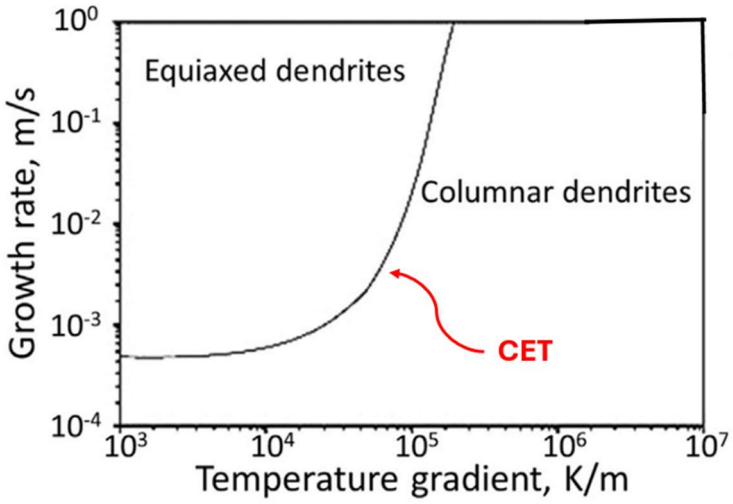

Figure 24: CET in a R vs G plot

This transition stage has been studied by J.D. Hunt [47], who showed how the CTE is commonly observed for most metallic alloys at constant G^n /R values, with the exponent n being a material-specific constant that varies depending on the alloy (n = 3.4 for steel). Drawing on this theoretical framework, later studies published by Lekakh et al. [36] found that $G^{3.4}/R$ values in a range of 10^3 to 10^4 [$K \cdot s \cdot m^{-2}$] are low enough to transition the CET

and induce the formation of equiaxed grains in austenitic stainless steel. *Figure 21* represents the above explained.

For comparative reasons, a study performed by Umberto Scipioni et al [35] on the cellular microstructure stability of 316L steel in LPBF, resulted in $G^{3.4}/R$ values in all of the different experiments performed (various processing parameters) within the range of 10^9 to 10^{10} [$K \cdot s \cdot m^{-2}$], which are several orders of magnitude superior to the previously determined critical value for CET in the alloy. Thus, possibly explaining why equiaxed grains are very unlikely observed in L-PBF-processed 316L samples, whereas columnar morphology is the common solidification pattern.

This resulted are backed by more recent separate studies performed by Nathalie et al. [25], whose research on defect optimization and microstructure analysis of LPBF 316L stainless steel concluded that the cooling rates where estimated (based on the same theoretical framework and analytical solutions as the other studies) between 10^5 and 10^7 [$K \cdot s \cdot m^{-2}$], which despite being lower, still rise well above the validated critical CET. As a clarification, the lower values obtained in [25] are coherent with the linear relationship between G/R to laser power over scan speed (linear energy density) established in [35], since the values of linear energy density used in Nathalie et al experimentation were also lower.

A final graph presented in the published study of Mukherjee et al. [48], shown in *Figure 22*, displays a temperature gradient and growth rate solidification map for DED-GMA, DED-L (other additive manufacturing processes) and most relevant to this study, LPBF manufactured 316L stainless steel samples [49, 50, 51] results on concrete experimental G and R values.

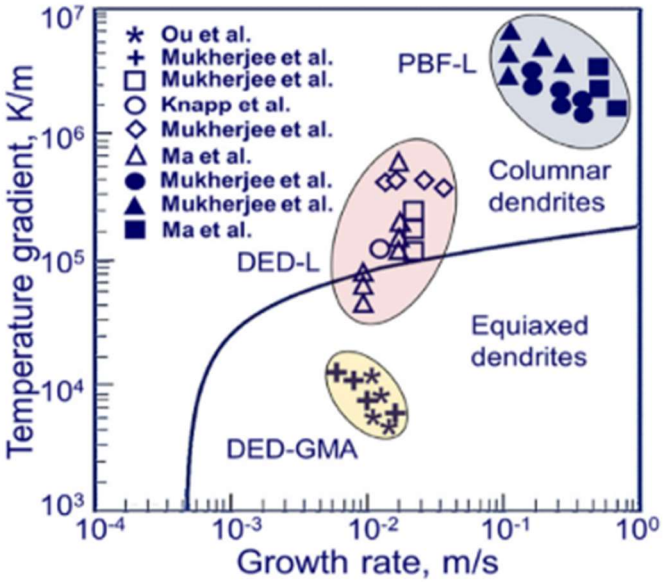

Figure 25: G vs R solidification map [48]

In other to avoid anisotropy derived from the columnar morphology and its property constraints, post-processing treatments such as heat aneling have been proven to be more effective than processing parameter manipulation, given the inherently high G/R values of LPBF [52].

Other methods that have shown satisfactory results to achieve a transition from columnar grains to fine isotropous equiaxed grains include a complex high-intensity ultrasound compound in the manufacturing process [38] ; or the addition of a simpler modification: a high substrate plate initial temperature (1275 ºC, tested in commercially available electron beam melting (EBM) systems), which allowed Raghavan et al. [54] to achieve lower thermal gradient, and therefore lower G/R ratios, thus favoring spontaneous nucleation of equiaxed grains. Although most of the commonly available L-PBF machines only allow build plate preheat temperatures up to 200 °C, the AconityMICRO system has a maximum preheat capability of 1200 ºC [2] and therefore reaching CET may be achievable under these circumstances. However, such high preheat of the build plate would have uncertain consequences on the energy input on the powder bed, therefore it would invalidate the previous VED line and framework, and it is out of the scope of this project.

Chapter 7. RESULTS

This chapter aims to present a coherent and curated parameter set that minimizes part defects of 316L samples fabricated on the AconityMICRO, basing on the thorough examination of the literature relative to analogous LPBF processes previously discussed. Moreover, results will also be drawn regarding the prediction of the morphology and grain size of these specimens. Lastly, the results of the preparation of the three crucial steps for the proper manipulation and application of knowledge to the AconityMICRO will also be discussed.

7.1 DEFINITION OF VED RANGES FOR OPTIMAL BUILDS

The purpose of this section is to conclude with a set of values for the main parameters that have been studied (laser power, scan speed, layer thickness, and hatch spacing) and a combination of these that enables the future user of the AconityMICRO to: basing on previous studies and the characteristics of VED, select 20 different combinations of the main parameters that most likely correspond to the larger optimal window of operation, and (by the future fabrication and testing of samples) check its consistency and correlation with LOF defects, keyhole porosity, or optimal density. Three main studies are the refence, in order of publication:

In 2014, Kamath et al. [34] addresses the issue of previously published literature on density of 316L stainless steel not analyzing laser powers higher than 225 W. Given this, Kamath decided to study this topic with laser powers up to 400 W (which is of great interest to this study since that is the upper bound of the power range for the AconityMICRO). This experiment was carried out using the Concept Laser M2 system, with small laser spot size of 54 µm. The layer thickness was set to 30 µm, and the hatch spacing to 70 µm. A total of 24 samples were tested combining laser powers from 150 W to 400 W in intervals of 50, and scan speed of 1300 to 2200 mm/s. These specifications implied VED ranges of 44.64 to 100.25 J/mm^3, for which the samples lower than 60 J/mm^3 presented the lower density

(<94%) due to LOF defects, while for optimal samples over that VED value density was >97%, and higher than 98.5% for powers greater than 250 W (VED higher than 67 J/mm^3). The results obtained are shown in *Figure 23*:

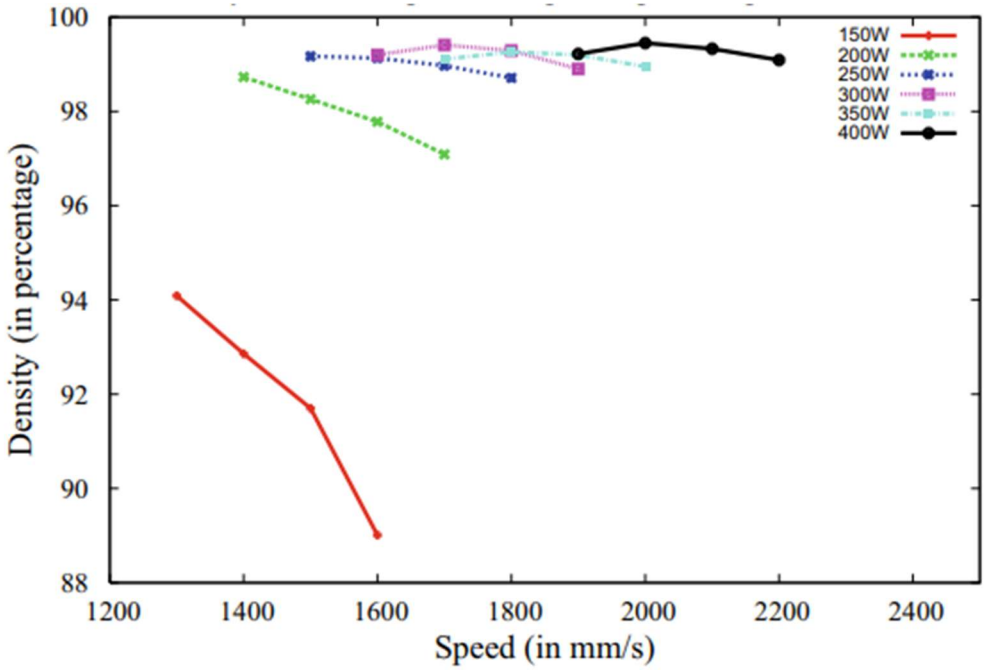

Figure 26: Density of samples tested by Kamath el al. [34]

A later relevant study was performed by Yakout et al. [24] in 2018. This paper, basing on the lack of clarity on how the choice of processing parameters and their relation affect part density in previous literature, it is the first to reference on VED ranges. The experiment includes a total of 27 samples of 316L stainless steel fabricated with the EOSINT M280 SLM system with a spot size of 80 µm, where layer thickness was set to 40 µm and hatch spacing varied between 0.080, 0.100, and 0.120 mm; in combination with laser power range of [200, 250, 300] W and scan speeds of [600, 800, 1000] mm/s. To determine the optimality of the samples, a series of mechanical and tensile tests were performed, with two determining energy transition parameters: a brittle-ductile-transition energy density (E_T) and critical laser energy density (E_C). Below E_T the parts exhibited void formation, low density, and brittle fracture (associated with insufficient energy input to the material or LOF). On the contrary, above E_C value, the parts showed excessive vaporization of elements (associated with

excessive energy input and keyholing dynamics). Stable melting ranges, and therefore optimal density samples were found for a VED range of 62.5 J/mm3 (E_T) to 104.2 J/mm^3 (E_C) as shown in *Figure 24*:

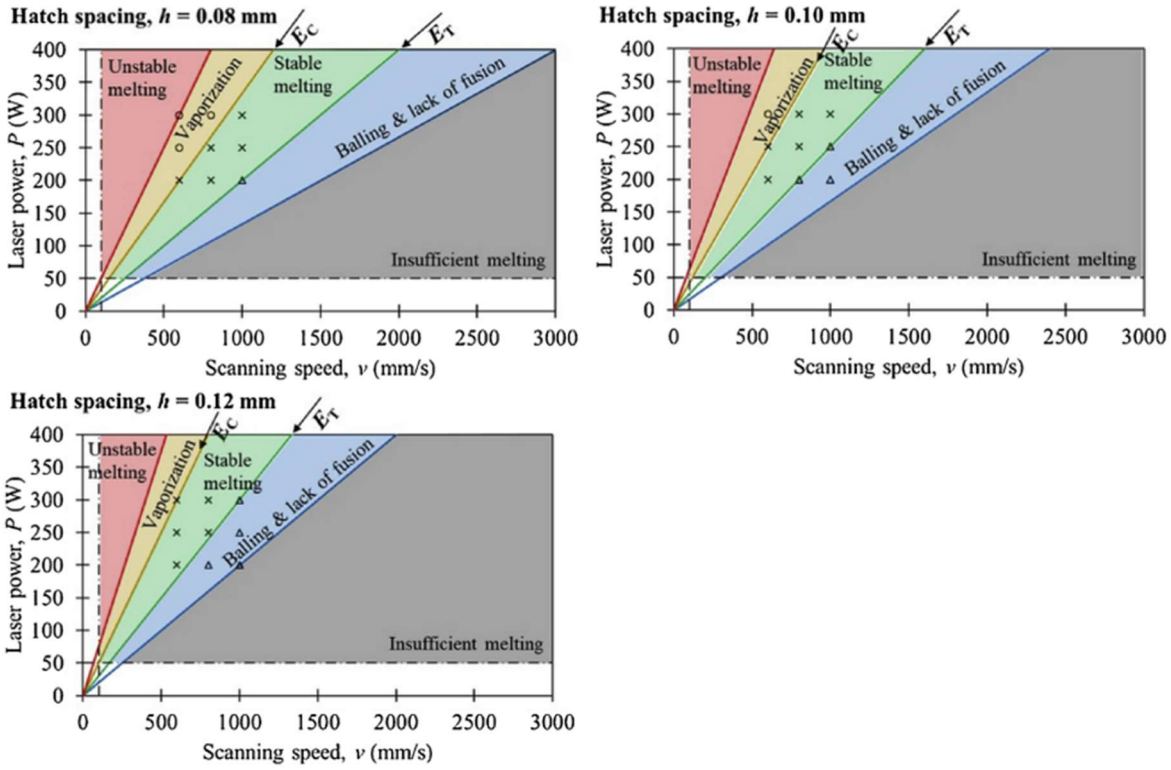

Figure 27: VED processing map results of Yakout et al. [24]

It is relevant to note that as hatch spacing increases, the defined areas in the plot shift towards smaller scan speeds and the windows are narrowed. A smaller hatch spacing provides the larger margin for optimal processing.

Lastly, in 2021, a more recent published work by Nathalie et al. [25] provides a comprehensive in depth understanding of the effect of the most influential LPBF parameters on density and defects, basing on the VED approach. It is the most specific literature piece on stainless steel 316L study of defects published. The SLM® 125HL system, with a laser spot size of 70 µm was used to fabricate 34 stainless steel 316L samples with fixed layer thickness and hatch spacing to 30 µm and 0.120 mm, respectively. Laser power values were

set at [125, 200, 275, 350] W in combination with scan speed ranging from 100 mm/s to 3400 mm/s as shown in *Figure 24*:

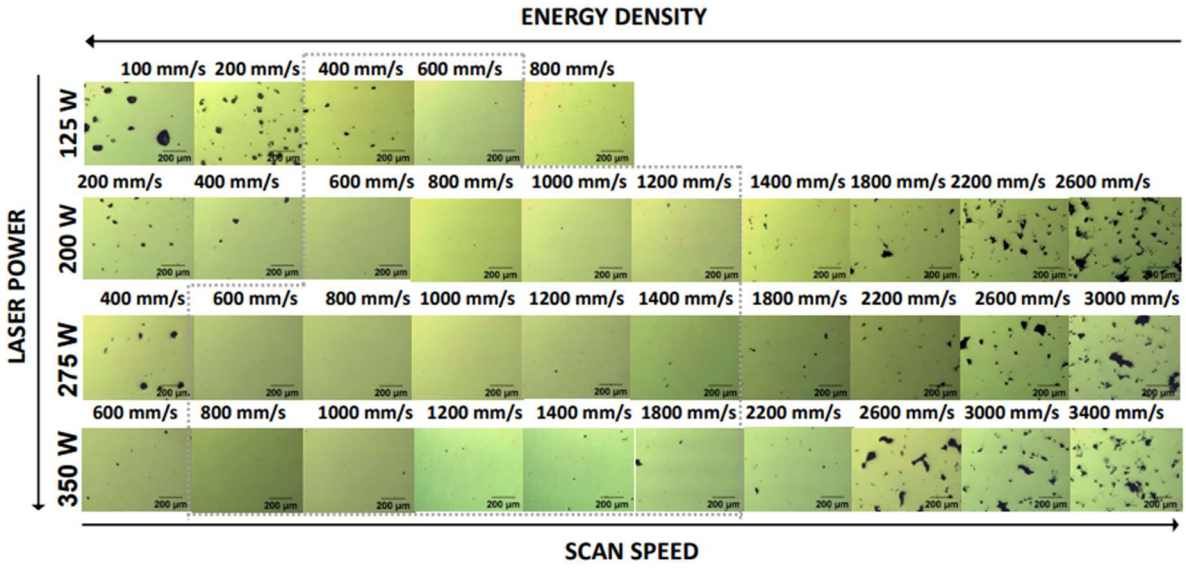

Figure 28: Optical micrographs from the cross-sections as function of P and V [25]

The dotted region in *Figure 24* with energy density values between 45 and 125 J/mm3 produced samples with density greater than 99.8% determined by image analysis. For the same sample testing, VED below 46 J/mm^3, yielded LOF defects as the fruit of insufficient melting, whereas excessive VED above 127 J/mm^3 resulted in keyhole porosity; compromising density to be lower than 98%.

In order to evaluate the three experimental studies and established a comprehensive comparison, a VED plot has been developed where the y-axis is still laser power [W], while the x-axis has been shifted from exclusively scan speed [mm/s], to the product of scan speed, layer thickness and hatch spacing (denominator of the energy density equation) in order to plot in the same graph data points with differences in the last two parameters. *Figure 25* represents all the data point in the three previously discussed studies where Set 1 corresponds to [25], Set 2 to [24], and Set 3 to [34], and the color scheme to LOF, keyhole, and optimal density, for blue, red and green, respectively.

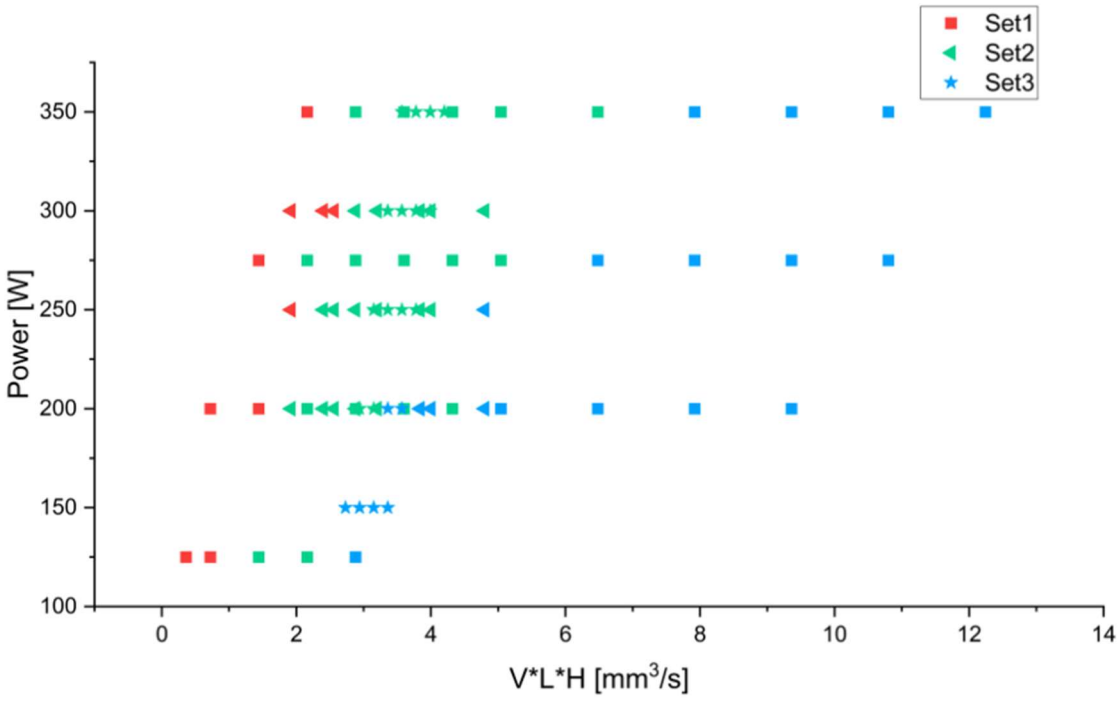

Figure 29: Plotting of most relevant literature references

The plot on *Figure 26* shows coherence between the different date points of the analyzed literature. There are two regions of overlap that could be simplified to: VED range between [100, 125] J/mm^3 coexistence of optimal density and keyhole porosity, with clear keyhole dynamics past above this range; a second overlap (specially for laser power below 200W) for VED ranges of [45, 65] J/mm^3 which translate into coexistence of optimality and LOF porosity, and clearly compromising defects below 45 J/mm^3. For all experiments on 316L studied, VED ranges between 65 and 100 J/mm^3 concentrated the highest density and therefore quality samples. Nonetheless, the exceptionally high density (>99.8%, porosity lower than 0.5%) samples present in Set 1 [25] in the discussed overlapped areas may suggest that significantly compromising porosity (above 2%) may not appear until VED under 30 J/mm^3 or above150 J/mm^3 are reached; additionally to the existence of transition zones from optimal density to high porosity for the ranges of 30 to 50 J/mm^3 (towards LOF) and 115 to 150 J/mm^3 (towards keyhole), respectively.

Basing on the research done in this study and the numerous papers' approaches to maximize part density; the influence of each the fundamental processing parameters on 316L stainless

steel LPBF builds, as well as taking into consideration the concrete specifications of the AconityMICRO system, the powder employed, and the recommended parameter values by the manufacturer; this present study asserts that a layer thickness of 30 µm and a hatch spacing of 0.080 mm (taken the small laser spot size of 40 µm) will most likely result in the largest optimal processing window. The VED Map present in annexed documents represents the expected optimality or defects for 316L parts fabricated with the AconityMICRO, following the reasoning developed in this section, and based on the energy density approach.

7.2 MICROSTRUCTURE CHARACTERISTICS EXPECTED UPON RESEARCH

The results discussed lead to the general conclusion that columnar grains are expected of 316L components manufactured by LPBF processes, including the AconityMICRO builds. Controlling microstructural morphology, specifically transitioning from columnar to equiaxed grains by reducing the G/R value below the critical CET, proved unfeasible for LPBF-processed 316L stainless steel solely through the adjustment of process parameters, as presented in the literature review. An extremely high substrate plate preheating (1200º C) in combination with the appropriate selection of laser power and scan speed may result in the formation of equiaxed grains but said processing environment exceeds this project's scope of work.

7.3 MANIPULATING THE ACONITYMICRO SYSTEM

As mentioned in the section regarding objectives of this project, three fundamental steps that should be taken on parallel to the density and microstructure study to ensure the proper operation of the machine and successful future research, have also been included in this project. As part of a rich preparation for any future scientific pursuits with the AconityMICRO, the assigned students of the research group at Cornell University fulfilled the following:

7.3.1 TRAINING SESSIONS BY INDUSTRY SPECIALISTS

A series of extensive training sessions were given to assigned students by an industry specialist sent by Aconity3D to the Grumman Laboratory located within Cornell University campus. On two separate occasions, between late March and early weeks of April of 2024, following the installation and set of the machine, these training sessions included:

I. Knowledge and manipulation of the surrounding technologies necessary for the smooth run of the AconityMICRO (argon gas supply, power, etc.), along with a safe start up and deactivation.
II. Basic familiarization with the AconityMICRO digital interface and operating software AconitySTUDIO, where students learned how to input a CAD model and its specific processing parameters, as well as starting and monitoring a build from beginning to end.
III. Appropriate powder manipulation, addition to the extractable powder cylinders, and posterior cleaning protocols.
IV. A practice build shown in *Figure 27*, where students followed all the necessary steps to ensure an independent, successful and responsible future use of the machine.

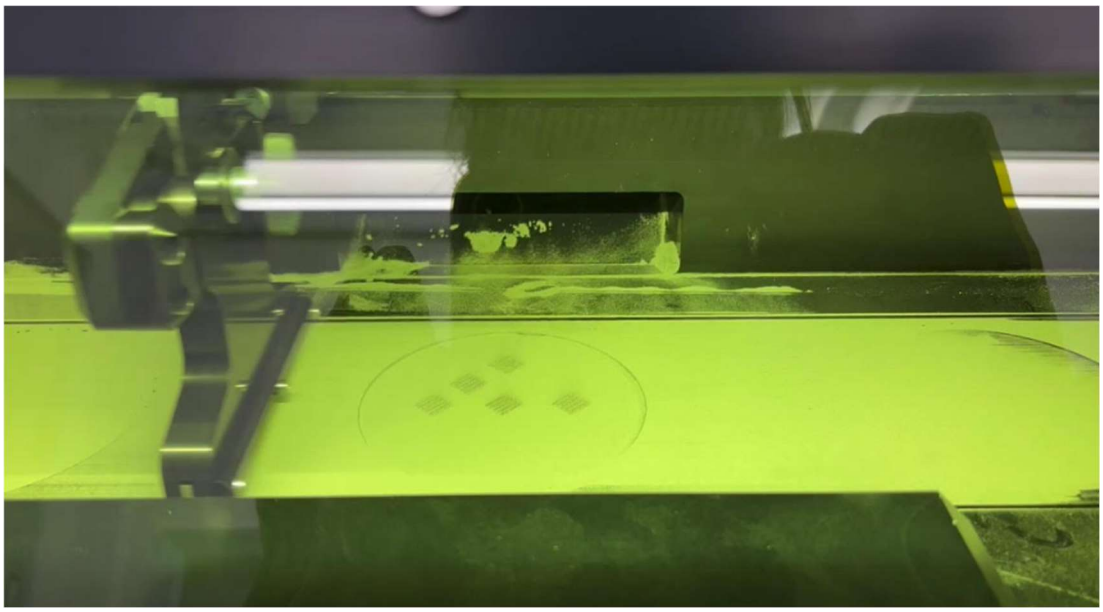

Figure 30: Practice build during training

7.3.2 NETFABB AND FUSION 360

Netfabb and Fusion 360 are two Autodesk software tools indispensable to design the CAD model that is posteriorly uploaded to the LPBF machine. The exact dimensions and geometry, along with the input part parameters are included in this model, and will be followed by the AconityMICRO operating software and consequently translated literally to the final part.

The minimum software skills necessary to fabricate geometrically simple components with the purpose of testing the effect of processing parameters and material properties are not complex. This project incorporated the familiarization with the Autodesk software in order to design 5x5x10 mm square structures (which are simple and easy to analyze and to apply post processing polishing and imaging on) with three pyramidal supports of 2.5 mm height. Once the structural component is designed in Fusion 360, it is transferred to Netfabb, where its location on the substrate plate can be determined along with the parameters associated with the component.

7.3.3 POST-PROCESSING PRACTICE

Once a build process has been completed, the excess powdered blown off and the substrate plate extracted, the components attached to the plate must be extracted. If the supports are correctly designed parts must not be difficult to remove and the substrate plane undamaged, following the extraction techniques taught during the training sessions.

A conventional post processing in order to analyze the density and microstructure of fabricated samples would include polishing and electronic optical microscopy imaging. As to practice proper polishing techniques and familiarizing with the image analysis, these post-processing procedures were practiced on other sample sets (previously manufactured by Aconity3D) at the Johnson Laboratory, under supervision of experienced students of the research group.

Chapter 8. CONCLUSIONS AND FUTURE WORK

In order to successfully produce a coherent set of components made of 316L stainless steel using the AconityMICRO LPBF machine located at Cornell University, the previously discussed results will serve as a guide and solid framework regarding defect and microstructure prediction. The most relevant analytical solutions and published studies have been carefully curated to obtain a comprehensive set of values for the critical processing parameters governing the LPBF builds, specific to the system and powdered material present at Cornell University. Basing on the energy density approach, the optimal processing window has been maximized to the fullest extent feasible, and a series of ranges of VED to predict defect formation have been provided. Additionally, sensible and literature-coherent assumptions have been made regarding microstructure development in these samples. Thus, the two main objectives of this project are fulfilled.

Regarding the steps ought to be made in parallel to assure the proper functioning and manipulation of the LPBF system by Aconity3D, the translation of information from CAD models to the machine's software, and the necessary post-processing procedures and skills have also been successfully completed, as stated in the results section. These are crucial for any future work with the machine.

Immediately following this project, before any future endeavors with the AconityMICRO, engineers may well aim to validate the accuracy and applicability of the previously established parameter maps derived from literature (accommodated to the specific equipment and powder acquired by Cornell). To pursue so, a series of samples may be built to verify the VED Map: Out of a total of 15 testing samples (a small number of pieces cognizant of the inexperience of a novel user of the AconityMICRO), it would be recommended to set 5 with parameters distributed along the optimal window, 4 distributed along the transition zones, and finally 6 along the areas most prone to defect appearance. A possible selection is shown in *Figure 28*, where a wide range of laser powers, scan speeds

and concrete VED values are targeted. Posterior analysis and comparison to expected results may be carried out.

POWER (W)								
400	666.67	333.33	222.22	166.67	133.33	111.11	95.24	83.33
375	625.00	312.50	208.33	156.25	125.00	104.17	89.29	78.13
350	583.33	291.67	194.44	145.83	116.67	97.22	83.33	72.92
325	541.67	270.83	180.56	135.42	108.33	90.28	77.38	67.71
300	500.00	250.00	166.67	125.00	100.00	83.33	71.43	62.50
275	458.33	229.17	152.78	114.58	91.67	76.39	65.48	57.29
250	416.67	208.33	138.89	104.17	83.33	69.44	59.52	52.08
225	375.00	187.50	125.00	93.75	75.00	62.50	53.57	46.88
200	333.33	166.67	111.11	83.33	66.67	55.56	47.62	41.67
175	291.67	145.83	97.22	72.92	58.33	48.61	41.67	36.46
150	250.00	125.00	83.33	62.50	50.00	41.67	35.71	31.25
125	208.33	104.17	69.44	52.08	41.67	34.72	29.76	26.04
100	166.67	83.33	55.56	41.67	33.33	27.78	23.81	20.83
75	125.00	62.50	41.67	31.25	25.00	20.83	17.86	15.63
50	83.33	41.67	27.78	20.83	16.67	13.89	11.90	10.42
25	41.67	20.83	13.89	10.42	8.33	6.94	5.95	5.21
SCAN SPEED (mm/s)	250	500	750	1000	1250	1500	1750	2000

Figure 31: Selection of parameters for 15 sample testing

To successfully manufacture and analyze the results of these samples, the mentioned steps (familiarizing with the operation of the machine through training sessions, the design and model of the sample parts in Netfabb software and posterior transfer to AconitySTUDIO, as well as post-processing polishing and imaging) are indispensable.

Chapter 9. BIBLIOGRAPHY

[1] Engler Modic, E. (2018, March 12). Additive manufacturing orthopedic implants. Today's Medical Developments. Last accessed: 2024, July. https://www.todaysmedicaldevelopments.com/news/renishaw-additive-manufacturing-orthopedic-implants/

[2] Aconity 3D. https://aconity3d.com/products/aconity-micro/

[3] Gaikwad, A., Williams, R. J., de Winton, H., Bevans, B. D., Smoqi, Z., Rao, P., & Hooper, P. A. (2022). Multi phenomena melt pool sensor data fusion for enhanced process monitoring of laser powder bed fusion additive manufacturing. Materials & Design, 221, 110919.

[4] Autodesk Inc. Netfabb. https://www.autodesk.com/es/products/netfabb/overview?term=1-YEAR&tab=subscription

[5] Autodesk Inc. Fusion 360. https://www.autodesk.com/es/products/fusion-360/overview?term=1-YEAR&tab=subscription

[6] Allied High Tech Products Inc. MULTIPREP™ SYSTEM 12". https://www.alliedhightech.com/equipment/multiprep-polishing-system-12

[7] Cornell Center for Material Research. Instruments. https://www.ccmr.cornell.edu/instruments/olympus-bx51-w1f/

[8] Oliveira, J. P., LaLonde, A. D., & Ma, J. (2020). Processing parameters in laser powder bed fusion metal additive manufacturing. Materials & Design, 193, 108762.

[9] Agrawal, A. K., Rankouhi, B., & Thoma, D. J. (2022). Predictive process mapping for laser powder bed fusion: A review of existing analytical solutions. Current Opinion in Solid State and Materials Science, 26(6), 101024.

[10] Heiden, M. J., Jensen, S. C., Koepke, J. R., Saiz, D. J., Dickens, S. M., & Jared, B. H. (2022). Process and feedstock driven microstructure for laser powder bed fusion of 316L stainless steel. Materialia, 21, 101356.

[11] S. Kou, Welding Metallurgy, 2nd ed. John Wiley & Sons, Hoboken, NJ, 2003.

[12] Rometsch, P. A., Zhu, Y., Wu, X., & Huang, A. (2022). Review of high-strength aluminium alloys for additive manufacturing by laser powder bed fusion. Materials & Design, 219, 110779.

[13] Liu, Zhuangzhuang. Vanmeensel, Kim.Xie, Jianxin. (2024). Alloy design for laser powder bed fusion additive manufacturing: a critical review. Vol 6. International Journal of Extreme Manufacturing.

[14] Fang, Y., Zhang, Y., Kim, M., Kim, H., No, J., Duan, Z., Yuan, Q., & Suhr, J. (2022). An austenite-rich composite of stainless steels with high strength and favorable ductility via selective laser melting of a powder mixture. Materials Science and Engineering: A, 855, 143891.

[15] Eres-Castellanos, A., Santana, A., Sanz-Moral, L. M., Rementeria, R., Pascual, R. H., Serrano, M., Toda-Caraballo, I., Jimenez, J. A., Caballero, F. G., & Capdevila, C. (2022). High temperature performance of 316L steel reinforced by particle inoculation and processed by laser powder bed fusion. Journal of Materials Research and Technology, 21, 2375-2382.

[16] Dryepondt, S., Nandwana, P., Unocic, K. A., Kannan, R., Fernandez Zelaia, P., & List, F. A. (2022). High temperature high strength austenitic steel fabricated by laser powder-bed fusion. Acta Materialia, 231, 117876.

[17] Vock, Silvia. Kloeden, Burghardt. Kirchner, Alexander. Weissgaerber, Thomas. Kieback, Bernd. (2019). Progress in Additive Manufacturing. Vol. 4. Powders for powder bed fusion: a review

[18] Gordon, J. V., Narra, S. P., Cunningham, R. W., Liu, H., Chen, H., Suter, R. M., Beuth, J. L., & Rollett, A. D. (2020). Defect structure process maps for laser powder bed fusion additive manufacturing. Additive Manufacturing, 36, 101552.

[19] Shrestha, S., & Chou, K. (2022). Formation of keyhole and lack of fusion pores during the laser powder bed fusion process. *Manufacturing Letters, 32*, 19-23.

[20] Yang, X., Li, Y., & Li, B. (2023). Formation mechanisms of lack of fusion and keyhole-induced pore defects in laser powder bed fusion process: A numerical study. International Journal of Thermal Sciences, 188, 108221.

[21] Guo, L., Liu, H., Wang, H., Wei, Q., Xiao, Y., Tang, Z., Wu, Y., & Wang, H. (2023). Identifying the keyhole stability and pore formation mechanisms in laser powder bed fusion additive manufacturing. Journal of Materials Processing Technology, 321, 118153.

[22] Wang, Wenjia, Jinqiang Ning, and Steven Y. Liang. 2021. "Analytical Prediction of Balling, Lack-of-Fusion and Keyholing Thresholds in Powder Bed Fusion" Applied Sciences 11, no. 24: 12053.

[23] Ng, G.K.L., Jarfors, A.E.W., Bi, G. et al. (2009). Porosity formation and gas bubble retention in laser metal deposition. Appl. Phys. A 97, 641–649.

[24] Yakout, M., Elbestawi, M. A., & Veldhuis, S. C. (2019). Density and mechanical properties in selective laser melting of invar 36 and stainless steel 316L. Journal of Materials Processing Technology, 266, 397-420.

[25] Diaz Vallejo, N.; Lucas, C.; Ayers, N.; Graydon, K.; Hyer, H.;Sohn, Y. Process Optimization and Microstructure Analysis to Understand Laser Powder Bed Fusion of 316L Stainless Steel. Metals 2021,11, 832.

[26] Chowdhury, S., Yadaiah, N., Prakash, C., Ramakrishna, S., Dixit, S., Gupta, L. R., & Buddhi, D. (2022). Laser powder bed fusion: A state-of-the-art review of the technology, materials, properties & defects, and numerical modelling. Journal of Materials Research and Technology, 20, 2109-2172.

[27] Hyer, H. C., & Petrie, C. M. (2022). Effect of powder layer thickness on the microstructural development of additively manufactured SS316. Journal of Manufacturing Processes, 76, 666-674.

[28] Ziri, S., Hor, A. & Mabru, C. Combined effect of powder properties and process parameters on the density of 316L stainless steel obtained by laser powder bed fusion. Int J Adv Manuf Technol 120, 6187–6204 (2022).

[29] Kruth J, Badrossamay M, Yasa E, Deckers J, Thijs L, Van Humbeeck J (2010a) Part and material properties in selective laser melting of metals. In: Proceedings of the 16th international symposium on electromachining (ISEM XVI), Shanghai

[30] Yasa E (2011) Manufacturing by combining selective laser melting and selective laser erosion/laser re-melting. PhD thesis, Faculty of Engineering, Department of

Mechanical Engineering, Katholieke Universiteit Leuven, Heverlee (Leuven), available from Katholieke Universiteit Leuven

[31] Yasa E, Craeghs T, Badrossamay M, Kruth JP (2009) Rapid manufacturing research at the Catholic University of Leuven. In: RapidTech 2009: US-TURKEY workshop on rapid technologies, Istanbul

[32] Wang S, Liu Y, Shi W, Qi B, Yang J, Zhang F, Han D, Ma Y. (2017). Research on High Layer Thickness Fabricated of 316L by Selective Laser Melting. Materials (Basel).

[33] Leicht, A., Fischer, M., Klement, U. et al. Increasing the Productivity of Laser Powder Bed Fusion for Stainless Steel 316L through Increased Layer Thickness. J. of Materi Eng and Perform 30, 575–584 (2021).

[34] Kamath, C., El-dasher, B., Gallegos, G.F. et al. Density of additively-manufactured, 316L SS parts using laser powder-bed fusion at powers up to 400 W. Int J Adv Manuf Technol 74, 65–78 (2014).

[35] Scipioni Bertoli, U., MacDonald, B. E., & Schoenung, J. M. (2019). Stability of cellular microstructure in laser powder bed fusion of 316L stainless steel. Materials Science and Engineering: A, 739, 109-117.

[36] Lekakh, S.N., O'Malley, R.J., Emmendorfer, M.C., & Hrebec, B. (2017). Control of Columnar to Equiaxed Transition in Solidification Macrostructure of Austenitic Stainless Steel Castings. Isij International, 57, 824-832.

[37] Krakhmalev, P.; Fredriksson, G.; Svensson, K.; Yadroitsev, I.; Yadroitsava, I.; Thuvander, M.; Peng, R. (2018). Microstructure, Solidification Texture, and Thermal Stability of 316 L Stainless Steel Manufactured by Laser Powder Bed Fusion. *Metals*, *8*, 643.

[38] Todaro, C.J., Easton, M.A., Qiu, D., Zhang, D., Bermingham, M.J., Lui, E.W., Brandt, M., StJohn, D.H., & Qian, M. (2020). Grain structure control during metal 3D printing by high-intensity ultrasound. Nature Communications, 11.

[39] Charmi, A., Falkenberg, R., Ávila, L., Mohr, G., Sommer, K., Ulbricht, A., Sprengel, M., Saliwan Neumann, R., Skrotzki, B., & Evans, A. (2021). Mechanical

anisotropy of additively manufactured stainless steel 316L: An experimental and numerical study. Materials Science and Engineering: A, 799, 140154.

[40] Weaver, J. and Rosenthal, I. (2021), Understanding Anisotropic Tensile Properties of Laser Powder Bed Fusion Additive Metals: A Detailed Review of Select Examples, Advanced Manufacturing Series (NIST AMS), National Institute of Standards and Technology, Gaithersburg, MD.

[41] Boettinger, W. J., Coriell, S. R., Greer, A. L., Karma, A., Kurz, W., Rappaz, M., & Trivedi, R. (2000). Solidification microstructures: Recent developments, future directions. Acta Materialia, 48(1), 43-70.

[42] Kou S. Welding Metallurgy. 2nd ed. New York: John Wiley; 2003.

[43] Trapp, J., Rubenchik, A. M., Guss, G., & Matthews, M. J. (2017). In situ absorptivity measurements of metallic powders during laser powder-bed fusion additive manufacturing. Applied Materials Today, 9, 341-349.

[44] Rubenchik, A. M., King, W. E., & Wu, S. S. (2018). Scaling laws for the additive manufacturing. Journal of Materials Processing Technology, 257, 234-243.

[45] Mills, K. C. (2002). Recommended values of thermophysical properties for selected commercial alloys. Woodhead publishing.

[46] DebRoy, T., Wei, H. L., Zuback, J. S., Mukherjee, T., Elmer, J. W., Milewski, J. O., Beese, A. M., Wilson-Heid, A., De, A., & Zhang, W. (2018). Additive manufacturing of metallic components – process, structure and properties. Progress in Materials Science, 92, 112-224.

[47] Hunt, J. D. (1984). Steady state columnar and equiaxed growth of dendrites and eutectic. Materials Science and Engineering, 65(1), 75-83.

[48] Mukherjee, T., & DebRoy, T. (2019). A digital twin for rapid qualification of 3D printed metallic components. Applied Materials Today, 14, 59-65.

[49] Mukherjee, T., Wei, H. L., De, A., & DebRoy, T. (2018). Heat and fluid flow in additive manufacturing – part II: Powder bed fusion of stainless steel, and titanium, nickel and aluminum base alloys. Computational Materials Science, 150, 369-380.

[50] Scipioni Bertoli, U., Guss, G., Wu, S., Matthews, M. J., & Schoenung, J. M. (2017). In-situ characterization of laser-powder interaction and cooling rates

through high-speed imaging of powder bed fusion additive manufacturing. Materials & Design, 135, 385-396.

[51] Ma, M., Wang, Z., & Zeng, X. (2017). A comparison on metallurgical behaviors of 316L stainless steel by selective laser melting and laser cladding deposition. Materials Science and Engineering: A, 685, 265-273.

[52] Bedmar, J., García-Rodríguez, S., Roldán, M., Torres, B., & Rams, J. (2022). Effects of the heat treatment on the microstructure and corrosion behavior of 316 L stainless steel manufactured by laser powder bed fusion. Corrosion Science, 209, 110777.

[53] Raghavan, N., Dehoff, R., Pannala, S., Simunovic, S., Kirka, M., Turner, J., Carlson, N., & Babu, S. S. (2016). Numerical modeling of heat-transfer and the influence of process parameters on tailoring the grain morphology of IN718 in electron beam additive manufacturing. Acta Materialia, 112, 303-314.

ANNEX I

ALIGNMENTS WITH THE SUSTAINABLE DEVELOPMENT GOALS:

The United Nations have presented a series of Sustainable Development Goals (SDG) which serve as a comprehensive framework designed to address global challenges and promote a sustainable atmosphere across social, economic, and environmental perspectives. A project based on the use of a Laser Powder Bed Fusion additive manufacturing machine to test 316L stainless steel parts can potentially align with several of these 17 SDG, ordered by decreasing correlation as follows:

Goal 9: Industry, Innovation, and Infrastructure

LPBF technology is at the forefront of AM innovation, revolutionizing how industries produce and design parts. More specifically, this technology allows for the creation of intricate and complex geometries that traditional manufacturing methods are not capable of reproducing, therefore contributing to advancing the industrial processes.

Goal 12: Responsible Consumption and Production

LPBF promotes responsible production by significantly reducing material waste. Unlike other manufacturing processes where excess material is often discarded, LPBF adds material layer by layer, optimizing its usage and minimizing waste. Moreover, 316L stainless Steel is a durable and recyclable material that aligns with sustainable production practices.

Goal 13: Climate Action

Additive manufacturing technologies like LPBF play a role in climate action by reducing energy consumption and greenhouse gas emissions compared to more traditional manufacturing methods. By adopting LPBF for testing stainless steel parts, this project indirectly favors climate action goals by promoting a more eco-friendly process.

Goal 14: Life Below Water and **Goal 15: Life on Land**

Whilst the connection between LPBF and terrestrial and marine ecosystems (specially) may not be obvious at first glance, sustainable manufacturing practices always contribute to protecting both life on land and below water. By reducing waste and optimizing resource utilization (preserving land resources by reducing deforestation and environmental degradation), LPBF helps mitigate environmental pollution and other harmful activities that affect both marine as well as terrestrial ecosystems.

Goal 17: Partnerships for the Goals

Collaboration and partnerships are essential for achieving sustainable development objectives. This project, involving the use of LPBF technology, represents a collaborative effort between industry, academia, and the scientific research community, by working together to innovate and implement sustainable manufacturing practices.

ANNEX II

The present VED based chart modeling the defect prediction for values of Power [W] and Scan Speed [mm/s], and fixed values for layer thickness and hatch spacing of 30 µm and 0.080 mm, respectively.

Optimal Range

Transition to Lack of Fusion

Significant LOF

Transition to Keyhole

Significant Keyhole

POWER (W)														
400	666.67	333.33	222.22	166.67	133.33	111.11	95.24	83.33	74.07	66.67	60.61	55.56	51.28	47.62
375	625.00	312.50	208.33	156.25	125.00	104.17	89.29	78.13	69.44	62.50	56.82	52.08	48.08	44.64
350	583.33	291.67	194.44	145.83	116.67	97.22	83.33	72.92	64.81	58.33	53.03	48.61	44.87	41.67
325	541.67	270.83	180.56	135.42	108.33	90.28	77.38	67.71	60.19	54.17	49.24	45.14	41.67	38.69
300	500.00	250.00	166.67	125.00	100.00	83.33	71.43	62.50	55.56	50.00	45.45	41.67	38.46	35.71
275	458.33	229.17	152.78	114.58	91.67	76.39	65.48	57.29	50.93	45.83	41.67	38.19	35.26	32.74
250	416.67	208.33	138.89	104.17	83.33	69.44	59.52	52.08	46.30	41.67	37.88	34.72	32.05	29.76
225	375.00	187.50	125.00	93.75	75.00	62.50	53.57	46.88	41.67	37.50	34.09	31.25	28.85	26.79
200	333.33	166.67	111.11	83.33	66.67	55.56	47.62	41.67	37.04	33.33	30.30	27.78	25.64	23.81
175	291.67	145.83	97.22	72.92	58.33	48.61	41.67	36.46	32.41	29.17	26.52	24.31	22.44	20.83
150	250.00	125.00	83.33	62.50	50.00	41.67	35.71	31.25	27.78	25.00	22.73	20.83	19.23	17.86
125	208.33	104.17	69.44	52.08	41.67	34.72	29.76	26.04	23.15	20.83	18.94	17.36	16.03	14.88
100	166.67	83.33	55.56	41.67	33.33	27.78	23.81	20.83	18.52	16.67	15.15	13.89	12.82	11.90
75	125.00	62.50	41.67	31.25	25.00	20.83	17.86	15.63	13.89	12.50	11.36	10.42	9.62	8.93
50	83.33	41.67	27.78	20.83	16.67	13.89	11.90	10.42	9.26	8.33	7.58	6.94	6.41	5.95
25	41.67	20.83	13.89	10.42	8.33	6.94	5.95	5.21	4.63	4.17	3.79	3.47	3.21	2.98
SCAN SPEED (mm/s)	250	500	750	1000	1250	1500	1750	2000	2250	2500	2750	3000	3250	3500

ANNEX III

CARPENTER ADDITIVE®

PowderRange

Test Certificate

CT POWDERRANGE 316LF Rev4

Batch 0001083630

Gas Atomised 316L Stainless Steel LPBF (Flexible)

For more information on Safety Data Sheets please contact:
MSDS@CarpenterAdditive.com

CHEMICAL ANALYSIS

		Units	Min	Max	Result	Approved
C	Carbon	weight %	0	0.030	0.016	Pass
Cr	Chromium	weight %	16.0	18.0	17.9	Pass
Fe	Iron	weight %	Balance	-	Balance	Pass
Mn	Manganese	weight %	0	2.00	0.83	Pass
Mo	Molybdenum	weight %	2.00	3.00	2.38	Pass
Ni	Nickel	weight %	10.0	14.0	12.7	Pass
N	Nitrogen	weight %	0	0.10	0.10	Pass
O	Oxygen	weight %	0	0.10	0.02	Pass
P	Phosphorus	weight %	0	0.045	0.008	Pass
Si	Silicon	weight %	0	1.00	0.59	Pass
S	Sulphur	weight %	0	0.030	0.005	Pass

SIEVE ANALYSIS - ASTM B214

	Units	Min	Max	Result	Approved
+63 µm	weight %	0	0	0	Pass
+53 µm	weight %	0	1	0	Pass
+45 µm	weight %	Info Only	-	0	Pass

LASER SIZE DIFFRACTION - ASTM B822

	Units	Min	Max	Result	Approved
Dv (10)	µm	Info Only	-	18.0	Pass
Dv (50)	µm	Info Only	-	31.0	Pass
Dv (90)	µm	Info Only	-	48.0	Pass
-5 µm	volume %	0	0	0	Pass
-16 µm	volume %	0	10	5	Pass

Carpenter Additive is a business unit of Carpenter Technology Corporation, LPW is a wholly owned subsidiary of CarpenterTechnology Corporation.
LPW Technology Limited is a company registered in England and Wales
Company Registeration: 06233481 VAT Registration Number: GB 920134667
Registered Office: 54 Portland Place London W1B 1DY

CARPENTER ADDITIVE®

PowderRange

Test Certificate

CT POWDERRANGE 316LF Rev4

Batch 0001083630

Gas Atomised 316L Stainless Steel LPBF (Flexible)

For more information on Safety Data Sheets please contact:
MSDS@CarpenterAdditive.com

HALL FLOW - ASTM B213

	Units	Min	Max	Result	Approved
FR_H	s/50g	Flow	-	16	Pass

APPARENT DENSITY - ASTM B212

	Units	Min	Max	Result	Approved
Bulk Density	g/cm³	Info Only	-	4.54	Pass

NOTES

We hereby certify that this materal has been produced, tested and inspected in accordance with customer purchase order and referenced specifications and conforms requirements.

*This document is validated by suppliers authorised inspection representative in accordance with EN 10204 type 3.1 Inspection Document

Material meets the requirements of CT POWDERRANGE 316LF

Approved By	Jonathan Latta		11/05/2023
Authorised By	Maria Sawford		11/05/2023

Carpenter Additive is a business unit of Carpenter Technology Corporation, LPW is a wholly owned subsidiary of CarpenterTechnology Corporation.
LPW Technology Limited is a company registered in England and Wales
Company Registeration: 06233481 VAT Registration Number: GB 920134667
Registered Office: 54 Portland Place London W1B 1DY